

# An Efficient Phase-Transition Framework for Gate-Tunable Superconductivity in Monolayer WTe<sub>2</sub>

F. Yang,<sup>1,\*</sup> G. D. Zhao,<sup>1</sup> Y. Shi,<sup>1</sup> and L. Q. Chen<sup>1,†</sup>

<sup>1</sup>Department of Materials Science and Engineering and Materials Research Institute,  
The Pennsylvania State University, University Park, PA 16802, USA

(Dated: September 11, 2025)

The recently reported gate-tunable superconductivity in monolayer WTe<sub>2</sub> [Science **362**, 922 (2018); Science **362**, 926 (2018); Nat. Phys. **20**, 269 (2023); PRR **7**, 013224 (2025)] exhibits several striking anomalies beyond the standard paradigm, including a contrasting carrier-density dependence of the transition temperature  $T_c$  in weakly and strongly disordered regimes and more surprisingly, the sudden disappearance of superconducting fluctuations below a critical carrier density. To understand these features, we go beyond the mean-field theory to treat the superconducting gap and superfluid density by explicitly incorporating both Nambu–Goldstone (NG) phase fluctuations and Berezinskii–Kosterlitz–Thouless (BKT) fluctuations. We show that these fluctuations are minimal in the weak-disorder regime but become crucial under strong disorder, where the zero-temperature gap renormalized by NG quantum fluctuations becomes density-dependent while the BKT fluctuations drive the superconducting  $T_c$  below the gap-closing temperature. Simulations within this unified framework combining with the density-functional-theory input to account for the excitonic instability quantitatively reproduced nearly all key experimental observations in monolayer WTe<sub>2</sub>, providing a consistent understanding of reported anomalies.

**Introduction.**—Over the past few decades, advances in material synthesis and growth techniques have led to the discovery of numerous two-dimensional quantum materials. A particularly striking development is the observation of superconductivity [1, 2], not only in conventional superconducting (SC) metals [3–8] and high- $T_c$  materials [9–13] realized as ultrathin films and atomic sheets but also in strictly monolayer (ML) transition-metal dichalcogenides such as MoS<sub>2</sub> [14–17], WTe<sub>2</sub> [18–21] and NbSe<sub>2</sub> [22–25]. These unique ML systems often exhibit unconventional and intriguing phenomena beyond the standard paradigm. A notable example is the recently reported ML WTe<sub>2</sub> [18–21], which displays an unusual set of anomalies: gate-tunable superconductivity with contrasting carrier-density dependence of the SC transition temperature  $T_c$  in weakly and strongly disordered regimes, and, most remarkably, a *sudden* disappearance of SC fluctuations below a critical doping. Such behaviors are in contrast to the mean-field BCS-theory description, which, for ML systems, predicts superconductivity independent of the carrier density and of the disorder (Anderson theorem) [26–29].

Physically, the reason why the ML SC systems are special is that they are fundamentally characterized by emerging SC-phase fluctuations, in contrast to the bulk case where superconductivity is described solely by the SC gap within the mean-field theory. These fluctuations comprise the longitudinal Nambu–Goldstone (NG) phase fluctuations and the transverse Berezinskii–Kosterlitz–Thouless (BKT) fluctuations.

The NG phase fluctuations arise as collective gapless long-wavelength modes dictated by the NG theorem [30–33], following the spontaneous breaking of  $U(1)$  symmetry in superconductors [34, 35]. Such smooth bosonic excitations [36–43] tend to restore the broken symmetry, thereby driving thermodynamic instabilities of the SC state. Certain mechanisms can, in principle, circumvent this instability. In 3D superconductors, the NG mode is gapped by the Anderson–Higgs mechanism [34, 35, 41, 44, 45] via long-range Coulomb interactions, which shift the original gapless spectrum to high-frequency

plasma energy  $\omega_p$ , suppressing phase fluctuations entirely. The same mechanism renormalizing the NG-mode dispersion to  $\omega_p$  also operates in ML superconductors, as demonstrated by early [39, 46–48] and recent [41, 42] theoretical studies on phase-mode spectrum. While  $\omega_p$  also becomes gapless in ML with a sublinear dispersion  $\omega_p(q) \propto \sqrt{q}$ , this form is expected to avoid the infrared divergence of phase correlations at finite  $T$  [41], providing a clear route to evade the Hohenberg–Mermin–Wagner–Coleman theorem [49–51], which forbids true long-range SC order in ML systems. Nevertheless, the gapless nature implies that the NG mode remains an active excitation which, while not yet fully resolved, is expected to play an essential role in renormalizing the SC gap [40–42, 52], in contrast to the dynamically inert case in 3D.

On the other hand, BKT fluctuations (i.e., vortex–antivortex excitations) [37, 53, 54] arise due to the discrete symmetry of phase transformation. These topological excitations/defects, which cannot be continuously deformed into the SC ground state, produce a universal discontinuous jump in the superfluid stiffness [55, 56], thereby driving the SC transition temperature  $T_c$  below the gap-closing temperature  $T_{\text{os}}$  and creating a phase-incoherent pairing regime above  $T_c$  [52, 57, 58]. In this case, the SC-normal transition at  $T_c$  is governed by the loss of long-range phase coherence rather than by the BCS closing of the pairing gap. The standard BKT renormalization-group (RG) approach requires the bare superfluid density as input, typically obtained from Ginzburg–Landau expression [37, 59] or the limiting form of BCS theory [52, 55]. This direct input may face challenges in disordered case [60–63], since it does not account for the disorder effect owing to the disorder-insensitivity predicted by the Anderson theorem [26–29]. In reality, ML materials, due to their reduced dimensionality, are intrinsically more susceptible to disorder, and experiments on strongly disordered ultra-thin films [57, 58, 64–70] have demonstrated that increasing the disorder suppresses  $T_c$ .

The ML SC system therefore simultaneously hosts fermionic quasiparticles, bosonic NG phase modes, BKT topological ex-

citations, and disorder. Existing theoretical approaches usually address these ingredients separately in the limiting form, while current computational methods (such as DMFT [71]) are optimized mainly for fermionic quasiparticles and are not well suited for treating different degrees of freedom on an equal footing. Here, we combine these ingredients in a self-consistent manner and apply the purely microscopic framework to ML WTe<sub>2</sub>. Specifically, starting from a microscopic model, we treat the SC gap by explicitly and self-consistently incorporating the bosonic excitation of NG phase mode (i.e., NG quantum and thermal phase fluctuations) in the presence of long-range Coulomb interactions, and calculate the disorder-influenced superfluid density, which serves as a physically consistent input to the BKT-model RG equation. This enables a unified description of phase dynamics and fermionic quasiparticles, offering a self-consistent phase-transition theory.

Applied to ML WTe<sub>2</sub>, our simulations show that both NG and BKT fluctuations are negligible in the weakly disordered regime, owing to the small electron effective mass. In contrast, under strong disorder, NG quantum phase fluctuations renormalize the zero-temperature gap into a density-dependent value, while BKT fluctuations drive the SC transition temperature  $T_c$  below the gap-closing temperature  $T_{\text{os}}$ , producing a large density-dependent separation  $T_{\text{os}} - T_c$ . NG thermal phase fluctuations remain negligible due to the long-range Coulomb interactions. Incorporating density-functional-theory (DFT) input and taking into account the excitonic instability, we quantitatively reproduce the key experimental observations of the gate-tunable superconductivity in ML WTe<sub>2</sub> [18–21], offering a consistent understanding of the reported anomalies.

*SC model.*—We begin with the standard microscopic Hamiltonian for *s*-wave superconductors (see Supplement Materials). The SC order parameter is written as  $\Delta = |\Delta| e^{i\delta\theta(\mathbf{R})}$ , with  $|\Delta|$  and  $\delta\theta(\mathbf{R})$  being the SC gap and phase, respectively. The phase fluctuation is defined as  $\mathbf{p}_s = \nabla_{\mathbf{R}}\delta\theta(\mathbf{R})/2$ . The phase dynamics  $\mathbf{p}_s$  can be decomposed into two orthogonal components [37]: the longitudinal  $\mathbf{p}_{s,\parallel}$  one, associated with NG long-wavelength (smooth) phase fluctuations, and the transverse  $\mathbf{p}_{s,\perp}$  one, corresponding to BKT vortex fluctuations (topological defects). The NG phase fluctuations, acting as a SC momentum [30, 33–35], are expected to renormalize the SC gap [40–42, 52], in a gauge manner analogous to the way a vector potential can influence the SC gap [30, 33, 34]. The resulting SC gap equation then reads

$$\frac{1}{U} = F(p_{s,\parallel}^2, |\Delta|, T) = \sum_{\mathbf{k}} \frac{f(E_{\mathbf{k}}^+) - f(E_{\mathbf{k}}^-)}{2E_{\mathbf{k}}}, \quad (1)$$

where phase fluctuations enter through the Doppler shift  $\mathbf{v}_{\mathbf{k}} \cdot \mathbf{p}_{s,\parallel}$  [42, 72–75] in the Bogoliubov quasiparticle energies  $E_{\mathbf{k}}^{\pm} = \mathbf{v}_{\mathbf{k}} \cdot \mathbf{p}_{s,\parallel} \pm E_{\mathbf{k}}$  with  $E_{\mathbf{k}} = \sqrt{\xi_{\mathbf{k}}^2 + |\Delta|^2}$ . Here,  $U$  stands for the pairing potential and  $v_{\mathbf{k}} = \partial_{\mathbf{k}}\xi_{\mathbf{k}}$  denotes the group velocity.  $\xi_{\mathbf{k}} = \hbar^2 k^2 / (2m_e) - E_F$  with  $E_F$  being the fermi energy (measured from the conduction-band minimum) and  $m_e$  being the effective mass of electron.  $f(x)$  is the Fermi distribution function. The SC gap equation here is an even function of the

phase fluctuations, and hence, influenced by the average [42]:

$$p_{s,\parallel}^2 = \langle p_{s,\text{NG}}^2 \rangle = \int \frac{d\mathbf{q}}{(2\pi)^2} \frac{q^2 [2n_B(\omega_{\text{NG}}) + 1]}{2D_q\omega_{\text{NG}}(q)}, \quad (2)$$

which is a standard bosonic excitation of the NG mode. The energy spectrum of NG mode is derived as  $\omega_{\text{NG}}(q) = \sqrt{n_s q^2 / (2D_q m)}$  with  $D_q = D / (1 + 2DV_q)$ , as established in the literature [34, 38–42, 45, 76]. Here,  $m$ ,  $D$  and  $V_q = 2\pi e^2 / (q\epsilon_0)$  denote the effective mass, density of states of carriers and 2D Coulomb potential, respectively. As is well established, the bosonic excitations  $2n_B(\omega_{\text{NG}}) + 1$  can be classified into the thermal excitations  $2n_B(x)$  and zero-point (quantum) oscillations, where  $n_B(x)$  is the Bose distribution function.

The superfluid density is obtained from the current–current correlation function, and written as

$$\frac{n_s}{n} = \frac{1}{1 + \xi/l} \int d\xi_k \int \frac{d\theta_{\mathbf{k}}}{2\pi} \frac{|\Delta|^2}{2E_{\mathbf{k}}^3} [f(E_{\mathbf{k}}^-) - f(E_{\mathbf{k}}^+)]. \quad (3)$$

Here, a prefactor  $(1 + \xi/l)^{-1}$  is included to account for disorder effects, where  $\xi = \hbar v_F / |\Delta|$  is the SC coherence length and  $l = v_F \gamma^{-1}$  is the mean free path, with  $\gamma$  representing the effective scattering rate, encompassing the quasiparticle decay and transport processes, and implicitly including the localization effects [62, 63, 66–70] in the disordered regime. This interpolation was originally introduced by Tinkham in the context of the penetration depth  $\lambda$  of *s*-wave superconductors [77], leading to  $\lambda^2 = \lambda_{\text{clean}}^2 (1 + \xi/l)$  and hence  $n_s \rightarrow n_s / (1 + \xi/l)$ . It is consistent with the Mattis–Bardeen result in the dirty limit [78, 79] and its subsequent extension to arbitrary scattering strength [80], and has been formulated in various approaches like Gorkov equation [81], Eilenberger equation [82–84], and gauge-invariant kinetic equation [75], as well as diagrammatic formulations incorporating *vertex* corrections to the current–current correlation [83, 85]. This approximation captures the essential suppression of the superfluid density by nonmagnetic disorder and possible localization effects, and shows that disorder affects the SC state only through the renormalization of  $n_s$  in the current–current correlation function, without directly modifying the gap equation for *s*-wave pairing, in accordance with Anderson’s theorem [26–29].

By self-consistently solving the gap equation, NG phase-fluctuations and superfluid density (see Supplement Materials for details), we obtain a bare superfluid density  $n_s$  that incorporates the effects of both fermionic quasiparticles and bosonic NG phase fluctuations as well as disorder effect. This bare superfluid density  $n_s$  serves as the input to the standard BKT RG approach [37, 54, 86–88]:

$$\frac{dK}{dl} = -K^2 g^2 \quad \text{and} \quad \frac{dg}{dl} = (2 - K)g, \quad (4)$$

where  $K(l = 0) = \frac{\pi\hbar^2 n_s}{4m_e k_B T}$  and  $g(l = 0) = 2\pi e^{-cK(l=0)}$  with the dimensionless constant  $c = 2/\pi$  in the ML limit [37]. This yields a renormalized value  $\bar{n}_s = \frac{4m_e k_B T}{\pi\hbar^2} K(l = \infty)$ , which further accounts for the vortex-antivortex fluctuations. The

SC transition temperature  $T_c$  is determined from the condition  $\bar{n}_s(T_c) = 0$  while the gap-closing temperature is denoted  $T_{os}$ . The factor  $n_s/m_e$  represents the phase stiffness, as established in numerous experiments [89–92]. A reduction of  $n_s/m_e$  lowers the excitation energy  $\omega_{NG}$  and bare coupling constant  $K(l=0)$  and hence enhances both NG and BKT fluctuations.

*Excitonic instability.*—The ML WTe<sub>2</sub> typically crystallizes in distorted 1T'-phase orthorhombic structure [93–95]. The band-structure calculations [93, 96] together with ARPES measurements [96] reveal that its Fermi surface consists of two electron pockets located near the  $\pm\mathbf{Q}$  points along the  $\Gamma$ –X direction and one hole pocket at the  $\Gamma$  point, originating from band inversion between W 5d and Te 5p orbitals. The carrier density can be continuously tuned via electrostatic gating [18–21, 97, 98]. However, due to the negative band gap  $E_g < 0$ , hole states emerge once the Fermi level  $E_F$  is lowered below  $|E_g|$ , and such holes can pair with electrons to form an excitonic insulator phase [98–100], which competes with superconductivity. In ML WTe<sub>2</sub>, the excitonic condensate is known to be sufficiently strong to dominate over the electron SC channel [18–21, 98]. This introduces an unequal competition between two distinct many-body states for conduction electrons [21]. To model this competition, we assume that each hole binds with one conduction electron to form an exciton, thereby depleting the electrons available for SC pairing. The effective density of states entering the electron-SC gap equation and the superfluid density is consequently reduced by a factor  $(n_e - n_h)/n_e$ . Here,  $n_e = 2n$  is the total conduction-band electron density and  $n_h$  is the hole density, both set by  $E_F$  and  $E_g$  in a parabolic-band 2DEG approximation.

*Results.*—The effective masses of electrons and holes are obtained from our DFT calculations [Fig. 2(a)]. While  $E_g$  can in principle be computed within DFT, its value should be sample dependent and sensitive to external conditions [101], and we treat it as a tunable parameter. The framework involves two tunable parameters that vary from sample to sample: the band gap  $E_g$  and the effective scattering rate  $\gamma$ . We first examine the density regime  $n_e \in [1, 2.8] \times 10^{13} \text{ cm}^{-2}$ , where holes are absent or negligible and superconductivity is therefore unaffected by the excitonic instability (set by  $E_g$ ).

In this density range and under weak disorder,  $T_{os}$  [orange solid curve in Fig. 1(a)] and the zero-temperature gap  $|\Delta(0)|$  [small  $\gamma$  in Fig. 1(d)] remain nearly density independent, so that the behavior essentially follows the mean-field description and NG fluctuations are negligible. This is consistent with the general conclusion that NG-fluctuation corrections to the gap are minimal in the clean limit [40]. The transition temperature  $T_c$  [orange dashed curve in Fig. 1(a)] shows only a faint density dependence; consequently, the difference between  $T_c$  and  $T_{os}$  is nonzero but small, as seen in the orange curves of Fig. 1(a) or in small- $\gamma$  case of Fig. 1(e), suggesting weak BKT fluctuations. The suppression of fluctuations originates from the small electron effective mass,  $m_e = 0.33m_0$  (from our DFT calculations, consistent with the experimental estimate  $m_e = 0.3m_0$  [19]), and the relatively high carrier density. Together, these yield a large phase stiffness  $n_s/m_e$ , which suppresses fluctuations.

In contrast, under strong disorder, where the superfluid density and thus the phase stiffness are strongly suppressed, fluctuations become significant. As shown in Fig. 1(c), BKT fluctuations at elevated temperatures cause the renormalized  $\bar{n}_s$  to decrease more rapidly than the bare value, ultimately leading to a discontinuous drop of the superfluid density and driving the SC transition at  $T_c$ , with  $T_c$  pushed significantly below the gap-closing temperature  $T_{os}$ . This creates a pseudogap (phase-incoherent pairing) regime in the window  $T_c < T < T_{os}$ , where pairing persists without the global phase coherence necessary to achieve superconductivity (zero-resistivity phenomenon). As a result, a large difference between  $T_c$  and  $T_{os}$  emerges under strong disorder and becomes more pronounced as density (phase stiffness) decreases, as shown by brown curves in Fig. 1(a), or in large- $\gamma$  case in Fig. 1(e).

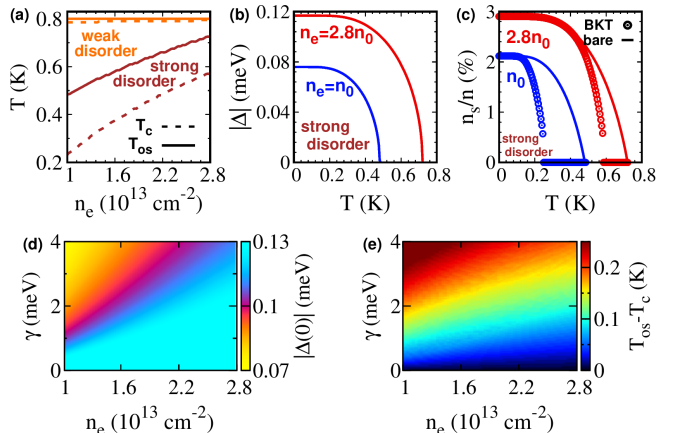


FIG. 1. Simulation results of superconductivity in ML WTe<sub>2</sub> at relatively high carrier density. (a)  $T_c$  (dashed) and  $T_{os}$  (solid) for weak disorder ( $\gamma = 0.12 \text{ meV}$ ) and strong disorder ( $\gamma = 3.2 \text{ meV}$ ). (b) Temperature dependence of the SC gap under strong disorder ( $\gamma = 3.2 \text{ meV}$ ) at two different densities. (c) Bare (curve) and BKT-renormalized (circles) superfluid density corresponding to the results in panel (b). (d, e) Zero-temperature gap  $|\Delta(0)|$  and the temperature difference  $T_{os} - T_c$  versus density and disorder, respectively. The pairing potential is fixed and specified in the Supplemental Materials.

On the other hand, we find that the zero-temperature gap  $|\Delta(0)|$  [Fig. 1(b),(d)], and consequently the gap-closing temperature  $T_{os}$  [brown solid curve in Fig. 1(a)] and the disorder-influenced superfluid-density ratio  $n_s(0)/n$  [Fig. 1(c)], acquire a clear dependence on both density and disorder under strong disorder, decreasing as the density (phase stiffness) is reduced or disorder is enhanced. Such SC-gap behavior under strong disorder is fully consistent with the STM and transport measurements on ML NbSe<sub>2</sub> [67, 102]. This emerging dependence arises from the enhanced NG quantum fluctuations (bosonic zero-point oscillations) by disorder-suppressed phase stiffness, which couple back into the SC gap equation and renormalize  $|\Delta(0)|$  in the strong-disorder case, unlike the mean-field and conventional BKT descriptions in 2D case, where the SC gap remains insensitive to density variation and disorder.

Nevertheless, we find that the NG thermal fluctuations re-

main minimal even under strong disorder, owing to the minimal thermal excitations of the NG mode  $n_B(\omega_{\text{NG}})$ . This arises from the change of the NG-mode energy spectrum from  $\omega_{\text{NG}}(q) \propto q$  to  $\omega_{\text{NG}}(q) \propto \sqrt{q}$  after accounting for the long-range Coulomb interactions, which confines low-energy excitations to a narrow momentum window with limited phase space. As a result, these modes propagate rapidly and are only weakly thermally populated, unlike acoustic-phonon-like linear modes, so their contributions to thermodynamics and critical dynamics become negligible. As proposed in Ref. [41, 42], this behavior represents an expected route to evade the infrared divergence of phase-fluctuation correlations at  $T \neq 0$  imposed by the Hohenberg–Mermin–Wagner–Coleman theorem [49–51]. As a result, although the zero-temperature gap is renormalized by NG bosons in a density- and disorder-dependent manner [Fig. 1(d)], its temperature evolution nevertheless follows the BCS-theory description, as shown in Fig. 1(b).

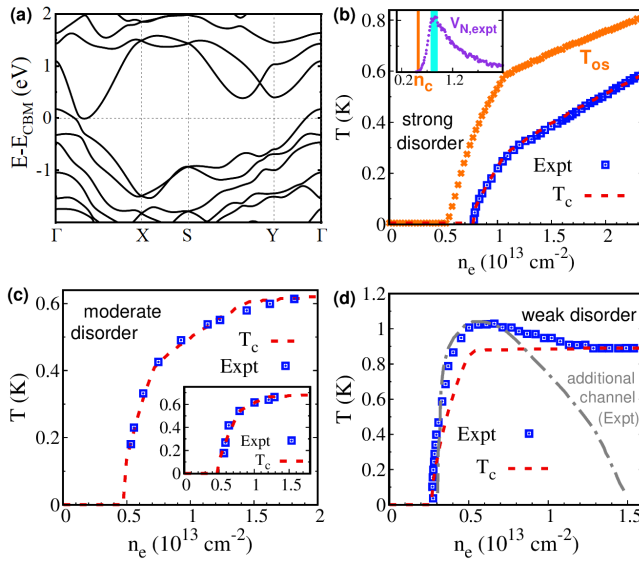


FIG. 2. (a) DFT calculation of the band structure of ML WTe<sub>2</sub>. (b), (c), inset of (c) and (d): experimentally measured  $T_c$  from Refs. [20], [18], [19] and [21], respectively, compared with our calculated  $T_c$  (dashed curves) obtained by fitting  $E_g$  and disorder strength. Crosses in (b) denote our calculated  $T_{\text{os}}$ . Inset of (b): experimentally measured Nernst signal  $V_n$  ( $T = 45$  mK,  $H = 23$  mT) in Ref. [20]. The orange line marks our calculated  $n_c$  where  $T_{\text{os}}$  vanishes, and the light blue region indicates the regime where our  $T_{\text{os}} - T_c$  [Fig. 3(b)] is maximized. The chain curve in (d) is extracted from the experimentally observed superconductivity that survives at  $H = 50$  mT [21].

After establishing the high-density behavior, we proceed to compare with experiments. The band gap  $E_g$  is adjusted to reproduce the experimentally observed critical density (quantum critical point) for the onset of superconductivity, while the disorder strength  $\gamma$  is determined from the high-density gap behavior discussed above. With these parameters fixed, as shown in Fig. 2, our framework quantitatively reproduces the experimentally observed density dependence of  $T_c$  in ML WTe<sub>2</sub>, and naturally accounts for the contrasting  $T_c$ –density

trends observed across four different samples in the literature.

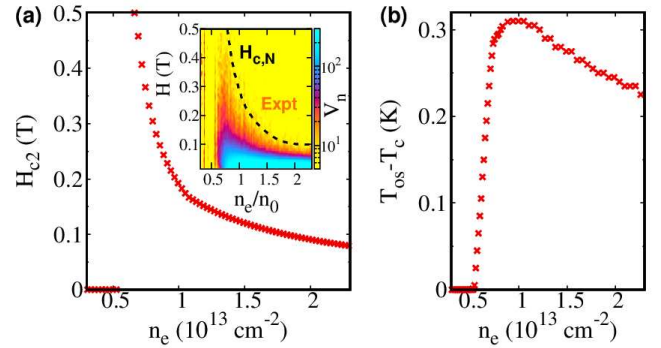


FIG. 3. Calculation of (a) the critical field  $H_{c2}(0)$  and (b) the temperature dependence of  $T_{\text{os}} - T_c$  as a function of density, corresponding to simulation in Fig. 2(b). Inset of (a): experimentally measured Nernst signal  $V_n$  ( $T = 45$  mK) (in unit of mV) from Ref. [20]; the dashed line indicates the field at which the signal vanishes in experiment.

Specifically, as shown in Fig. 2(a), the experimental data of Ref. [20] exhibit a pronounced density dependence of  $T_c$  in the high-density regime, consistent with a strong-disorder scenario. Across the entire density range, our calculated  $T_c(n)$  (dashed curve) nearly coincides with the experimental data (blue squares). Notably, the Nernst-signal measurements at a fixed magnetic field in Ref. [20] (purple dots in the inset of Fig. 2(a)) reveal a sudden disappearance of SC fluctuations below a critical density  $n_c$ . In our framework, this abrupt disappearance is naturally explained by the vanishing of  $T_{\text{os}}$ , signaling the termination of superconductivity by the excitonic instability. The density value  $n_p$  at which the measured Nernst signal peaks is associated with the density where  $T_{\text{os}} - T_c$  in our calculation is maximized [Fig. 3(b)], identifying the regime of strongest fluctuations. The measured critical magnetic field  $H_{c,n}$  [inset of Fig. 3(a)], at which the Nernst signal vanishes in the low- $T$  limit, corresponds to  $H_{c2}(0) = \frac{\pi m^2 |\Delta(0)|^2 \Phi_0}{8\pi^4 n_s(0)}$  in our calculation, above which Cooper pairs are fully suppressed. Remarkably, as shown in the inset of Fig. 2(b) and in Fig. 3(a), our predicted results, without adjustable parameters, accurately reproduce the experimental values of  $n_c$ ,  $n_p$ , and, in particular,  $H_{c,n}$ , and its divergence-like dependence of as the density decreases [103], in a quantitative agreement.

The experimental data of Ref. [18] [Fig. 2(c)] and Ref. [19] [inset of Fig. 2(c)] exhibit a weak yet visible density dependence of  $T_c$  in the high-density range, consistent with a moderate-disorder scenario, and our calculated  $T_c(n)$  closely follows the experimental trend across entire density range.

The recently reported experimental data of Ref. [21] show only minimal density variation of  $T_c$  in the high-density range, consistent with a weak-disorder scenario. In this case, our results quantitatively capture the density independence of  $T_c$  at high densities ( $n_e > 1 \times 10^{13}/\text{cm}^2$ ) and qualitatively describes its rapid suppression as the excitonic instability is approached ( $n_e < 0.5 \times 10^{13}/\text{cm}^2$ ), as shown in Fig. 2(d). However, in this sample a small anomalous upturn of  $T_c$  appears within the

density range  $n_e \in (0.5, 1) \times 10^{13} \text{ cm}^{-2}$ , where  $T_c$  increases upon reducing  $n_e$ , deviating from our theoretical curve.

Experimental observation of this anomalous upturn remain scarce, so far limited to the study in Ref. [21]. It could be a measurement artifact (e.g., electrostatic screening or device geometry), but it may also suggest the presence of an additional SC pairing channel active in this density window. In experiment [21], upon gradually applying an external magnetic field that selectively suppresses the background SC component, with the suppression setting in first on the high-density side, the visibility of the low-density SC behavior is enhanced. As a result, the residual  $T_c$  exhibits a distinct  $T_c$ – $n_e$  dome behavior, as indicated by the gray chain curve in Fig. 2(d) (extracted from the 50 mT data); the dome sharpens at larger fields and persists up to  $\sim 250$  mT. In this case, as seen in Fig. 2(d), combining this field-robust additional-channel  $T_c$  with our calculated background  $T_c$  (red dashed curve), i.e., taking the larger of the two (short-circuit effect), reproduces the experimentally measured zero-field  $T_c(n)$  (blue squares).

The additional SC channel could arise from an unconventional electron–electron pairing channel emerging near an excitonic instability [104]. Alternatively, it may stem from a hole-sector SC contribution on the electron-doped side, yielding a multiband superconductivity akin to  $\text{MgB}_2$ , since the relatively low critical density  $n_c$  for SC state reported in Ref. [21] implies an incomplete participation of the hole Fermi surface in the excitonic condensate. Owing to band inversion in ML WTe<sub>2</sub>, holes and electrons share similar orbital character on the electron-doped side, implying comparable pairing interactions and thus the potential for hole-SC state. Our DFT calculations find a large effective mass of hole,  $m_h = 0.53m_0$ . The resulting large density of states suggests that hole-SC pairing gap can be strong and may transiently overcome the excitonic competition in this density window. On the electron-doping side, the hole concentration remains low. This combination (low  $n_h$  and large  $m_h$ ) yields a notably small phase stiffness, making hole-SC state highly susceptible to disorder—suppressed under strong or moderate disorder, and emerging only under weak disorder where its  $T_c^h$  can exceed the electron-background  $T_c^e$ . The low  $n_h$ , large  $m_h$ , and a sizable SC gap also imply a shorter SC coherence length, making hole-SC state more robust against magnetic-field depairing, with  $H_{c2}^h$  expected to exceed  $H_{c2}^e$ . But it should be emphasized that this additional SC channel inferred on the electron-doped side under weak disorder is unlikely on the hole-doped side, where the orbital character differs and the absence of band inversion likely precludes the same pairing mechanism from forming [105].

A more complete understanding requires additional experiments and first-principles calculations to determine whether nontrivial competition among candidate many-body states exists. Accordingly, we confine the present work to the background SC component and the corresponding anomalies reported in the literature. In this context, using DFT input to incorporate excitonic instability, our framework that combines fermionic quasiparticles with phase dynamics to treat the SC gap and superfluid density in a self-consistent manner, quan-

titatively reproduced nearly all key experimental observations of the gate-tunable superconductivity in ML WTe<sub>2</sub> [18–20], offering a consistent understanding of the reported anomalies. The theory is general and can potentially be utilized to understand a broad range of SC phase transitions in ML systems.

The present study does not address calculations of the microscopic origin of the pairing potential, nor the reason why Zeeman depairing effect of magnetic fields is minimal. A quantitative assessment of these issues requires first-principles calculations of the electron–phonon interactions and the spin-related effect, respectively, as in Ref. [105] and Refs. [106, 107].

*Acknowledgments.*— This work is supported by the US Department of Energy, Office of Science, Basic Energy Sciences, under Award Number DE-SC0020145 as part of Computational Materials Sciences Program. F.Y. and L.Q.C. also appreciate the generous support from the Donald W. Hamer Foundation through a Hamer Professorship at Penn State.

---

\* fzy5099@psu.edu

† lqc3@psu.edu

- [1] Y. Saito, T. Nojima, and Y. Iwasa, Highly crystalline 2D superconductors, *Nat. Rev. Mater.* **2**, 1 (2016).
- [2] D. Qiu, C. Gong, S. Wang, M. Zhang, C. Yang, X. Wang, and J. Xiong, Recent advances in 2D superconductors, *Advanced Materials* **33**, 2006124 (2021).
- [3] C. Li, Y.-F. Zhao, A. Vera, O. Lesser, H. Yi, S. Kumari, Z. Yan, C. Dong, T. Bowen, K. Wang, *et al.*, Proximity-induced superconductivity in epitaxial topological insulator/graphene/gallium heterostructures, *Nat. Mater.* **22**, 570 (2023).
- [4] T. Zhang, P. Cheng, W.-J. Li, Y.-J. Sun, G. Wang, X.-G. Zhu, K. He, L. Wang, X. Ma, X. Chen, *et al.*, Superconductivity in one-atomic-layer metal films grown on Si(111), *Nat. Phys.* **6**, 104 (2010).
- [5] J. Falson, Y. Xu, M. Liao, Y. Zang, K. Zhu, C. Wang, Z. Zhang, H. Liu, W. Duan, K. He, *et al.*, Type-II Ising pairing in few-layer stanene, *Science* **367**, 1454 (2020).
- [6] M. Liao, Y. Zang, Z. Guan, H. Li, Y. Gong, K. Zhu, X.-P. Hu, D. Zhang, Y. Xu, Y.-Y. Wang, *et al.*, Superconductivity in few-layer stanene, *Nat. Phys.* **14**, 344 (2018).
- [7] H.-M. Zhang, Y. Sun, W. Li, J.-P. Peng, C.-L. Song, Y. Xing, Q. Zhang, J. Guan, Z. Li, Y. Zhao, *et al.*, Detection of a superconducting phase in a two-atom layer of hexagonal Ga film grown on semiconducting GaN(0001), *Phys. Rev. Lett.* **114**, 107003 (2015).
- [8] N. Briggs, B. Bersch, Y. Wang, J. Jiang, R. J. Koch, N. Nayir, K. Wang, M. Kolmer, W. Ko, A. De La Fuente Duran, *et al.*, Atomically thin half-van der waals metals enabled by confinement heteroepitaxy, *Nat. Mater.* **19**, 637 (2020).
- [9] Y. Yu, L. Ma, P. Cai, R. Zhong, C. Ye, J. Shen, G. D. Gu, X. H. Chen, and Y. Zhang, High-temperature superconductivity in monolayer  $\text{Bi}_2\text{Sr}_2\text{CaCu}_2\text{O}_{8+\delta}$ , *Nature* **575**, 156 (2019).
- [10] S. He, J. He, W. Zhang, L. Zhao, D. Liu, X. Liu, D. Mou, Y.-B. Ou, Q.-Y. Wang, Z. Li, *et al.*, Phase diagram and electronic indication of high-temperature superconductivity at 65 K in single-layer FeSe films, *Nat. Mater.* **12**, 605 (2013).
- [11] J. Lee, F. Schmitt, R. Moore, S. Johnston, Y.-T. Cui, W. Li, M. Yi, Z. Liu, M. Hashimoto, Y. Zhang, *et al.*, Interfacial mode

coupling as the origin of the enhancement of  $T_c$  in FeSe films on  $\text{SrTiO}_3$ , *Nature* **515**, 245 (2014).

[12] J.-F. Ge, Z.-L. Liu, C. Liu, C.-L. Gao, D. Qian, Q.-K. Xue, Y. Liu, and J.-F. Jia, Superconductivity above 100 K in single-layer FeSe films on doped  $\text{SrTiO}_3$ , *Nat. Mater.* **14**, 285 (2015).

[13] H. Ding, Y.-F. Lv, K. Zhao, W.-L. Wang, L. Wang, C.-L. Song, X. Chen, X.-C. Ma, and Q.-K. Xue, High-temperature superconductivity in single-unit-cell FeSe films on anatase  $\text{TiO}_2(001)$ , *Phys. Rev. Lett.* **117**, 067001 (2016).

[14] J. T. Ye, Y. J. Zhang, R. Akashi, M. S. Bahramy, R. Arita, and Y. Iwasa, Superconducting dome in a gate-tuned band insulator, *Science* **338**, 1193 (2012).

[15] J. Lu, O. Zheliuk, I. Leermakers, N. F. Yuan, U. Zeitler, K. T. Law, and J. Ye, Evidence for two-dimensional Ising superconductivity in gated  $\text{MoS}_2$ , *Science* **350**, 1353 (2015).

[16] Y. Saito, Y. Nakamura, M. S. Bahramy, Y. Kohama, J. Ye, Y. Kasahara, Y. Nakagawa, M. Onga, M. Tokunaga, T. Nojima, *et al.*, Superconductivity protected by spin-valley locking in ion-gated  $\text{MoS}_2$ , *Nat. Phys.* **12**, 144 (2016).

[17] D. Costanzo, S. Jo, H. Berger, and A. F. Morpurgo, Gate-induced superconductivity in atomically thin  $\text{MoS}_2$  crystals, *Nat. Nanotechnol.* **11**, 339 (2016).

[18] V. Fatemi, S. Wu, Y. Cao, L. Bretheau, Q. D. Gibson, K. Watanabe, T. Taniguchi, R. J. Cava, and P. Jarillo-Herrero, Electrically tunable low-density superconductivity in a monolayer topological insulator, *Science* **362**, 926 (2018).

[19] E. Sajadi, T. Palomaki, Z. Fei, W. Zhao, P. Bement, C. Olsen, S. Luescher, X. Xu, J. A. Folk, and D. H. Cobden, Gate-induced superconductivity in a monolayer topological insulator, *Science* **362**, 922 (2018).

[20] T. Song, Y. Jia, G. Yu, Y. Tang, P. Wang, R. Singha, X. Gui, A. J. Uzan-Narovlansky, M. Onyszczak, K. Watanabe, *et al.*, Unconventional superconducting quantum criticality in monolayer  $\text{WTe}_2$ , *Nat. Phys.* **20**, 269 (2024).

[21] T. Song, Y. Jia, G. Yu, Y. Tang, A. J. Uzan, Z. J. Zheng, H. Guan, M. Onyszczak, R. Singha, X. Gui, K. Watanabe, T. Taniguchi, R. J. Cava, L. M. Schoop, N. P. Ong, and S. Wu, Unconventional superconducting phase diagram of monolayer  $\text{WTe}_2$ , *Phys. Rev. Res.* **7**, 013224 (2025).

[22] J.-P. Xu, M.-X. Wang, Z. L. Liu, J.-F. Ge, X. Yang, C. Liu, Z. A. Xu, D. Guan, C. L. Gao, D. Qian, *et al.*, Experimental detection of a Majorana mode in the core of a magnetic vortex inside a topological insulator-superconductor  $\text{Bi}_2\text{Te}_3/\text{NbSe}_2$  heterostructure, *Phys. Rev. Lett.* **114**, 017001 (2015).

[23] H.-H. Sun, K.-W. Zhang, L.-H. Hu, C. Li, G.-Y. Wang, H.-Y. Ma, Z.-A. Xu, C.-L. Gao, D.-D. Guan, Y.-Y. Li, *et al.*, Majorana zero mode detected with spin selective Andreev reflection in the vortex of a topological superconductor, *Phys. Rev. Lett.* **116**, 257003 (2016).

[24] H. Wang, X. Huang, J. Lin, J. Cui, Y. Chen, C. Zhu, F. Liu, Q. Zeng, J. Zhou, P. Yu, *et al.*, High-quality monolayer superconductor  $\text{NbSe}_2$  grown by chemical vapour deposition, *Nat. Commun.* **8**, 394 (2017).

[25] A. Tsen, B. Hunt, Y. Kim, Z. Yuan, S. Jia, R. Cava, J. Hone, P. Kim, C. Dean, and A. Pasupathy, Nature of the quantum metal in a two-dimensional crystalline superconductor, *Nat. Phys.* **12**, 208 (2016).

[26] P. W. Anderson, Theory of dirty superconductors, *J. Phys. Chem. Solids* **11**, 26 (1959).

[27] H. Suhl and B. Matthias, Impurity scattering in superconductors, *Phys. Rev.* **114**, 977 (1959).

[28] S. Skalski, O. Betbeder-Matibet, and P. Weiss, Properties of superconducting alloys containing paramagnetic impurities, *Phys. Rev.* **136**, A1500 (1964).

[29] L. Andersen, A. Ramires, Z. Wang, T. Lorenz, and Y. Ando, Generalized Anderson's theorem for superconductors derived from topological insulators, *Sci. Adv.* **6**, eaay6502 (2020).

[30] Y. Nambu, Quasi-particles and gauge invariance in the theory of superconductivity, *Phys. Rev.* **117**, 648 (1960).

[31] J. Goldstone, Field theories with superconductor solutions, *Il Nuovo Cimento* **19**, 154 (1961).

[32] J. Goldstone, A. Salam, and S. Weinberg, Broken symmetries, *Phys. Rev.* **127**, 965 (1962).

[33] Y. Nambu, Nobel lecture: Spontaneous symmetry breaking in particle physics: A case of cross fertilization, *Rev. Mod. Phys.* **81**, 1015 (2009).

[34] V. Ambegaokar and L. P. Kadanoff, Electromagnetic properties of superconductors, *Il Nuovo Cimento* **22**, 914 (1961).

[35] P. Littlewood and C. Varma, Gauge-invariant theory of the dynamical interaction of charge density waves and superconductivity, *Phys. Rev. Lett.* **47**, 811 (1981).

[36] A. Paramekanti, M. Randeria, T. V. Ramakrishnan, and S. S. Mandal, Effective actions and phase fluctuations in d-wave superconductors, *Phys. Rev. B* **62**, 6786 (2000).

[37] L. Benfatto, *The Berezinskii-Kosterlitz-Thouless Transition and its Application to Superconducting Systems* (2024).

[38] L. Benfatto, A. Toschi, S. Caprara, and C. Castellani, Phase fluctuations in superconductors: From galilean invariant to quantum XY models, *Phys. Rev. B* **64**, 140506 (2001).

[39] L. Benfatto, A. Toschi, and S. Caprara, Low-energy phase-only action in a superconductor: A comparison with the XY model, *Phys. Rev. B* **69**, 184510 (2004).

[40] i. c. v. Kos, A. J. Millis, and A. I. Larkin, Gaussian fluctuation corrections to the bcs mean-field gap amplitude at zero temperature, *Phys. Rev. B* **70**, 214531 (2004).

[41] S. Fischer, M. Hecker, M. Hoyer, and J. Schmalian, Short-distance breakdown of the higgs mechanism and the robustness of the bcs theory for charged superconductors, *Phys. Rev. B* **97**, 054510 (2018).

[42] F. Yang and M. Wu, Theory of coupled dual dynamics of macroscopic phase coherence and microscopic electronic fluids: Effect of dephasing on cuprate superconductivity, *Phys. Rev. B* **104**, 214510 (2021).

[43] L. Benfatto, S. Caprara, C. Castellani, A. Paramekanti, and M. Randeria, Phase fluctuations, dissipation, and superfluid stiffness in d-wave superconductors, *Phys. Rev. B* **63**, 174513 (2001).

[44] P. W. Anderson, Plasmons, gauge invariance, and mass, *Phys. Rev.* **130**, 439 (1963).

[45] F. Yang and M. Wu, Gauge-invariant microscopic kinetic theory of superconductivity: Application to the optical response of Nambu-Goldstone and Higgs modes, *Phys. Rev. B* **100**, 104513 (2019).

[46] M. P. Fisher, G. Grinstein, and S. Girvin, Presence of quantum diffusion in two dimensions: Universal resistance at the superconductor-insulator transition, *Phys. Rev. Lett.* **64**, 587 (1990).

[47] M. P. Fisher, Quantum phase transitions in disordered two-dimensional superconductors, *Phys. Rev. Lett.* **65**, 923 (1990).

[48] T. Mishonov and A. Groshev, Plasmon excitations in josephson arrays and thin superconducting layers, *Phys. Rev. Lett.* **64**, 2199 (1990).

[49] P. C. Hohenberg, Existence of long-range order in one and two dimensions, *Phys. Rev.* **158**, 383 (1967).

[50] N. D. Mermin and H. Wagner, Absence of ferromagnetism or antiferromagnetism in one-or two-dimensional isotropic Heisenberg models, *Phys. Rev. Lett.* **17**, 1133 (1966).

[51] S. Coleman, There are no Goldstone bosons in two dimensions,

Commun. Math. Phys. **31**, 259 (1973).

[52] S. Mandal, S. Dutta, S. Basistha, I. Roy, J. Jesudasan, V. Bagwe, L. Benfatto, A. Thamizhavel, and P. Raychaudhuri, Destruction of superconductivity through phase fluctuations in ultrathin  $\alpha$ -moge films, Phys. Rev. B **102**, 060501 (2020).

[53] A. M. Goldman, The berezinskii–kosterlitz–thouless transition in superconductors, in *40 Years of Berezinskii–Kosterlitz–Thouless Theory*, pp. 135–160.

[54] J. B. Curtiss, N. Maksimovic, N. R. Poniatski, A. Yacoby, B. Halperin, P. Narang, and E. Demler, Probing the berezinskii–kosterlitz–thouless vortex unbinding transition in two-dimensional superconductors using local noise magnetometry, Phys. Rev. B **110**, 144518 (2024).

[55] A. Weitzel, L. Pfaffinger, I. Maccari, K. Kronfeldner, T. Huber, L. Fuchs, J. Mallord, S. Linzen, E. Il’ichev, N. Paradiso, and C. Strunk, Sharpness of the berezinskii–kosterlitz–thouless transition in disordered nbn films, Phys. Rev. Lett. **131**, 186002 (2023).

[56] G. Venditti, J. Biscaras, S. Hurand, N. Bergeal, J. Lesueur, A. Dogra, R. C. Budhani, M. Mondal, J. Jesudasan, P. Raychaudhuri, S. Caprara, and L. Benfatto, Nonlinear  $i$ – $v$  characteristics of two-dimensional superconductors: Berezinskii–kosterlitz–thouless physics versus inhomogeneity, Phys. Rev. B **100**, 064506 (2019).

[57] M. Chand, G. Saraswat, A. Kamlapure, M. Mondal, S. Kumar, J. Jesudasan, V. Bagwe, L. Benfatto, V. Tripathi, and P. Raychaudhuri, Phase diagram of the strongly disordered s-wave superconductor NbN close to the metal-insulator transition, Phys. Rev. B **85**, 014508 (2012).

[58] M. Mondal, A. Kamlapure, M. Chand, G. Saraswat, S. Kumar, J. Jesudasan, L. Benfatto, V. Tripathi, and P. Raychaudhuri, Phase fluctuations in a strongly disordered s-wave NbN superconductor close to the metal-insulator transition, Phys. Rev. Lett. **106**, 047001 (2011).

[59] B. I. Halperin and D. R. Nelson, Resistive transition in superconducting films, Journal of Low Temperature Physics **36**, 599 (1979).

[60] X.-C. Wang and Y. Qi, Phase fluctuations in two-dimensional superconductors and pseudogap phenomenon, Phys. Rev. B **107**, 224502 (2023).

[61] I. Maccari, L. Benfatto, and C. Castellani, Disordered xy model: Effective medium theory and beyond, Phys. Rev. B **99**, 104509 (2019).

[62] Z.-X. Li, S. A. Kivelson, and D.-H. Lee, Superconductor-to-metal transition in overdoped cuprates, npj Quantum Mater. **6**, 36 (2021).

[63] Y. Dubi, Y. Meir, and Y. Avishai, Nature of the superconductor-insulator transition in disordered superconductors, Nature **449**, 876 (2007).

[64] S. Chockalingam, M. Chand, J. Jesudasan, V. Tripathi, and P. Raychaudhuri, Superconducting properties and hall effect of epitaxial NbN thin films, Phys. Rev. B **77**, 214503 (2008).

[65] Y. Noat, V. Cherkez, C. Brun, T. Cren, C. Carobillet, F. Debontridder, K. Ilin, M. Siegel, A. Semenov, H.-W. Hübers, *et al.*, Unconventional superconductivity in ultrathin superconducting NbN films studied by scanning tunneling spectroscopy, Phys. Rev. B **88**, 014503 (2013).

[66] B. Sacépé, C. Chapelier, T. Baturina, V. Vinokur, M. Baklanov, and M. Sanquer, Disorder-induced inhomogeneities of the superconducting state close to the superconductor-insulator transition, Phys. Rev. Lett. **101**, 157006 (2008).

[67] B. Sacépé, M. Feigel’man, and T. M. Klapwijk, Quantum breakdown of superconductivity in low-dimensional materials, Nat. Phys. **16**, 734 (2020).

[68] B. Sacépé, T. Dubouchet, C. Chapelier, M. Sanquer, M. Ovadia, D. Shahar, M. Feigel’man, and L. Ioffe, Localization of preformed Cooper pairs in disordered superconductors, Nat. Phys. **7**, 239 (2011).

[69] D. Sherman, U. S. Pracht, B. Gorshunov, S. Poran, J. Jesudasan, M. Chand, P. Raychaudhuri, M. Swanson, N. Trivedi, A. Auerbach, *et al.*, The Higgs mode in disordered superconductors close to a quantum phase transition, Nat. Phys. **11**, 188 (2015).

[70] T. Dubouchet, B. Sacépé, J. Seidemann, D. Shahar, M. Sanquer, and C. Chapelier, Collective energy gap of preformed Cooper pairs in disordered superconductors, Nat. Phys. **15**, 233 (2019).

[71] Y. Shi, J. Schirmer, and L.-Q. Chen, Hall coefficient and resistivity in the doped bilayer hubbard model, Phys. Rev. B **109**, 075114 (2024).

[72] P. Fulde and R. A. Ferrell, Superconductivity in a strong spin-exchange field, Phys. Rev. **135**, A550 (1964).

[73] A. Larkin and Y. N. Ovchinnikov, Nonuniform state of superconductors, JETP **20**, 762 (1965).

[74] F. Yang and M. W. Wu, Fulde–Ferrell state in spin–orbit-coupled superconductor: Application to Dresselhaus SOC, J. Low Temp. Phys. **192**, 241 (2018).

[75] F. Yang and M. Wu, Gauge-invariant microscopic kinetic theory of superconductivity in response to electromagnetic fields, Phys. Rev. B **98**, 094507 (2018).

[76] Z. Sun, M. Fogler, D. Basov, and A. J. Millis, Collective modes and terahertz near-field response of superconductors, Phys. Rev. Res. **2**, 023413 (2020).

[77] M. Tinkham, *Introduction to superconductivity*, Vol. 1 (Courier Corporation, 2004).

[78] F. Yang and M. Wu, Diamagnetic property and optical absorption of conventional superconductors with magnetic impurities in linear response, Phys. Rev. B **109**, 064508 (2024).

[79] D. C. Mattis and J. Bardeen, Theory of the anomalous skin effect in normal and superconducting metals, Phys. Rev. **111**, 412 (1958).

[80] S. B. Nam, Theory of electromagnetic properties of superconducting and normal systems. I, Phys. Rev. **156**, 470 (1967).

[81] A. A. Abrikosov, L. P. Gorkov, and I. E. Dzyaloshinski, *Methods of quantum field theory in statistical physics* (Courier Corporation, 2012).

[82] G. Eilenberger, Transformation of gorkov’s equation for type ii superconductors into transport-like equations, Z. Phys. **214**, 195 (1968).

[83] M. Silaev, Nonlinear electromagnetic response and higgs-mode excitation in bcs superconductors with impurities, Phys. Rev. B **99**, 224511 (2019).

[84] K. D. Usadel, Generalized diffusion equation for superconducting alloys, Phys. Rev. Lett. **25**, 507 (1970).

[85] F. Yang and M. W. Wu, Impurity scattering in superconductors revisited: Diagrammatic formulation of the supercurrent-supercurrent correlation and higgs-mode damping, Phys. Rev. B **106**, 144509 (2022).

[86] L. Benfatto, C. Castellani, and T. Giamarchi, Broadening of the berezinskii–kosterlitz–thouless superconducting transition by inhomogeneity and finite-size effects, Phys. Rev. B **80**, 214506 (2009).

[87] L. Benfatto, C. Castellani, and T. Giamarchi, Doping dependence of the vortex-core energy in bilayer films of cuprates, Phys. Rev. B **77**, 100506 (2008).

[88] J. Yong, T. R. Lemberger, L. Benfatto, K. Ilin, and M. Siegel, Robustness of the berezinskii–kosterlitz–thouless transition in ultrathin nbn films near the superconductor-insulator transition,

Phys. Rev. B **87**, 184505 (2013).

[89] Y. Uemura, G. Luke, B. Sternlieb, J. Brewer, J. Carolan, W. Hardy, R. Kadono, J. Kempton, R. Kiefl, S. Kreitzman, *et al.*, Universal correlations between  $T_c$  and  $n_s/m^*$  (carrier density over effective mass) in high- $T_c$  cuprate superconductors, Phys. Rev. Lett. **62**, 2317 (1989).

[90] V. Emery and S. Kivelson, Importance of phase fluctuations in superconductors with small superfluid density, Nature **374**, 434 (1995).

[91] Y. Uemura, L. Le, G. Luke, B. Sternlieb, W. Wu, J. Brewer, T. Riseman, C. Seaman, M. Maple, M. Ishikawa, *et al.*, Basic similarities among cuprate, bismuthate, organic, Chevrel-phase, and heavy-fermion superconductors shown by penetration-depth measurements, Phys. Rev. Lett. **66**, 2665 (1991).

[92] O. Yuli, I. Asulin, O. Millo, D. Orgad, L. Iomin, and G. Koren, Enhancement of the superconducting transition temperature of  $\text{La}_{2-x}\text{Sr}_x\text{CuO}_4$  bilayers: Role of pairing and phase stiffness, Phys. Rev. Lett. **101**, 057005 (2008).

[93] X. Qian, J. Liu, L. Fu, and J. Li, Quantum spin hall effect in two-dimensional transition metal dichalcogenides, Science **346**, 1344 (2014).

[94] Z. Fei, T. Palomaki, S. Wu, W. Zhao, X. Cai, B. Sun, P. Nguyen, J. Finney, X. Xu, and D. H. Cobden, Edge conduction in monolayer  $\text{WTe}_2$ , Nature Physics **13**, 677 (2017).

[95] S.-Y. Xu, Q. Ma, H. Shen, V. Fatemi, S. Wu, T.-R. Chang, G. Chang, A. M. M. Valdivia, C.-K. Chan, Q. D. Gibson, J. Zhou, Z. Liu, K. Watanabe, T. Taniguchi, H. Lin, R. J. Cava, L. Fu, N. Gedik, and P. Jarillo-Herrero, Electrically switchable berry curvature dipole in the monolayer topological insulator  $\text{WTe}_2$ , Nature Physics **14**, 900 (2018).

[96] S. Tang, C. Zhang, D. Wong, Z. Pedramrazi, H.-Z. Tsai, C. Jia, B. Moritz, M. Claassen, H. Ryu, S. Kahn, J. Jiang, H. Yan, M. Hashimoto, D. Lu, R. G. Moore, C.-C. Hwang, C. Hwang, Z. Hussain, Y. Chen, M. M. Ugeda, Z. Liu, X. Xie, T. P. Devreux, M. F. Crommie, S.-K. Mo, and Z.-X. Shen, Quantum spin hall state in monolayer  $\text{WTe}_2$ , Nature Physics **13**, 683 (2017).

[97] S. Wu, V. Fatemi, Q. D. Gibson, K. Watanabe, T. Taniguchi, R. J. Cava, and P. Jarillo-Herrero, Observation of the quantum spin hall effect up to 100 kelvin in a monolayer crystal, Science **359**, 76 (2018).

[98] Y. Jia, P. Wang, C.-L. Chiu, Z. Song, G. Yu, B. Jäck, S. Lei, S. Klemenz, F. A. Cevallos, M. Onyszczak, N. Fishchenko, X. Liu, G. Farahi, F. Xie, Y. Xu, K. Watanabe, T. Taniguchi, B. A. Bernevig, R. J. Cava, L. M. Schoop, A. Yazdani, and S. Wu, Evidence for a monolayer excitonic insulator, Nature Physics **18**, 87 (2022).

[99] D. Jérôme, T. M. Rice, and W. Kohn, Excitonic insulator, Phys. Rev. **158**, 462 (1967).

[100] W. Kohn, Excitonic phases, Phys. Rev. Lett. **19**, 439 (1967).

[101] C. Zhao, M. Hu, J. Qin, B. Xia, C. Liu, S. Wang, D. Guan, Y. Li, H. Zheng, J. Liu, and J. Jia, Strain tunable semimetal-topological-insulator transition in monolayer  $\text{WTe}_2$ , Phys. Rev. Lett. **125**, 046801 (2020).

[102] K. Zhao, H. Lin, X. Xiao, W. Huang, W. Yao, M. Yan, Y. Xing, Q. Zhang, Z.-X. Li, S. Hoshino, J. Wang, S. Zhou, L. Gu, M. S. Bahramy, H. Yao, N. Nagaosa, Q.-K. Xue, K. T. Law, X. Chen, and S.-H. Ji, Disorder-induced multifractal superconductivity in monolayer niobium dichalcogenides, Nature Physics **15**, 904 (2019).

[103] This divergence-like density dependence of the critical field  $H_{c,n}(0)$  reported in Ref. [21] was attributed to an unconventional pairing channel, where the resulting SC gap  $|\Delta(0)|$  is assumed to increase at lower densities while  $T_c$  is suppressed, thereby implying a decoupling between the  $T_c$  and gap behaviors. This interpretation, however, relies on the assumption that superconductivity is destroyed solely by the Zeeman depairing effect of the magnetic field, i.e.,  $H_{c,n}(0) \propto |\Delta(0)|$ . Alternatively, our analysis suggests that in Nernst measurements the relevant threshold is the orbital depairing of magnetic field, yielding the scaling relation  $H_{c,n}(0) \propto |\Delta(0)|/n_s(0) \propto |\Delta(0)|(1 + \xi/l)/(2n_e - n_h)$ . This offers a natural explanation of the apparent divergence as approaching the critical density without requiring an unconventional pairing mechanism.

[104] V. Crépel and L. Fu, Spin-triplet superconductivity from excitonic effect in doped insulators, Proceedings of the National Academy of Sciences **119**, e2117735119 (2022).

[105] W. Yang, C.-J. Mo, S.-B. Fu, Y. Yang, F.-W. Zheng, X.-H. Wang, Y.-A. Liu, N. Hao, and P. Zhang, Soft-mode-phonon-mediated unconventional superconductivity in monolayer  $\text{WTe}_2$ , Phys. Rev. Lett. **125**, 237006 (2020).

[106] Y.-M. Xie, B. T. Zhou, and K. T. Law, Spin-orbit-parity-coupled superconductivity in topological monolayer  $\text{WTe}_2$ , Phys. Rev. Lett. **125**, 107001 (2020).

[107] Y.-T. Hsu, W. S. Cole, R.-X. Zhang, and J. D. Sau, Inversion-protected higher-order topological superconductivity in monolayer  $\text{WTe}_2$ , Phys. Rev. Lett. **125**, 097001 (2020).

# An Efficient Phase-Transition Framework for Gate-Tunable Superconductivity in Monolayer WTe<sub>2</sub> (Supplement Materials)

F. Yang,<sup>1,\*</sup> G. D. Zhao,<sup>1</sup> Y. Shi,<sup>1</sup> and L. Q. Chen<sup>1,†</sup>

<sup>1</sup>*Department of Materials Science and Engineering and Materials Research Institute, The Pennsylvania State University, University Park, PA 16802, USA*

(Dated: September 11, 2025)

## SI. Theoretical framework

The theoretical framework of the present work has been summarized in the main text. In this section, we introduce its fundamental derivation from the microscopic superconducting (SC) model. We start with the standard microscopic Hamiltonian of the *s*-wave superconductors [1–4]:

$$H_0 = \int d\mathbf{x} \left[ \sum_s \psi_s^\dagger(\mathbf{x}) \xi_{\hat{\mathbf{p}}} \psi_s(\mathbf{x}) - U \psi_\uparrow^\dagger(\mathbf{x}) \psi_\downarrow^\dagger(\mathbf{x}) \psi_\downarrow(\mathbf{x}) \psi_\uparrow(\mathbf{x}) \right] + \frac{1}{2} \sum_{ss'} \int d\mathbf{x} d\mathbf{x}' V(\mathbf{x} - \mathbf{x}') \psi_s^\dagger(\mathbf{x}) \psi_{s'}^\dagger(\mathbf{x}') \psi_{s'}(\mathbf{x}') \psi_s(\mathbf{x}). \quad (\text{S1})$$

Here,  $\psi_s^\dagger(\mathbf{x})$  and  $\psi_s(\mathbf{x})$  represent the creation and annihilation field operators of electron with spin  $s = \uparrow, \downarrow$ , respectively;  $U$  denotes the *s*-wave pairing potential;  $\xi_{\hat{\mathbf{p}}} = \frac{\hat{\mathbf{p}}^2}{2m} - E_F$  with  $\hat{\mathbf{p}} = -i\hbar\nabla$  being the momentum operator and  $E_F$  standing for the fermi energy;  $V(\mathbf{x} - \mathbf{x}')$  represents the long-range Coulomb. From the Hamiltonian, one can write down the action of this model and apply the Hubbard-Stratonovich transformation to obtain the action of superconductors. Then, by separating the center-of-mass [ $R = \frac{x_1+x_2}{2} = (t, \mathbf{R})$ ] and relative [ $r = x_1 - x_2 = (\tau, \mathbf{r})$ ] coordinates of the pairing electrons and following the standard treatment within the path-integral approach [4–8], the effective action of the gap and phase fluctuation is given by (the detailed derivation is addressed in Sec. SIA)

$$S_{\text{eff}} = \int dR \left\{ \sum_{p_n, \mathbf{k}} \ln[(ip_n - E_{\mathbf{k}}^+)(ip_n - E_{\mathbf{k}}^-)] - \frac{|\Delta|^2}{U} - \frac{np_s^2}{m} \right\} + \int dt \sum_{\mathbf{q}} \frac{D}{1+2DV_q} \left( \frac{\partial_t \delta\theta_{\mathbf{q}}}{2} \right)^2. \quad (\text{S2})$$

Here, the Doppler-shifted quasiparticle energy spectra  $E_{\mathbf{k}}^\pm = \mathbf{v}_{\mathbf{k}} \cdot \mathbf{p}_s \pm E_{\mathbf{k}}$  with  $E_{\mathbf{k}} = \sqrt{\xi_{\mathbf{k}}^2 + |\Delta|^2}$ ;  $p_n = (2n + 1)\pi T$  denotes the Fermion Matsubara frequency;  $\mathbf{k}$  and  $\mathbf{q}$  represent the momenta of Fermion and Boson that are transferred from the relative and center-of-mass spatial coordinates, respectively.

Through the variation  $\delta S_{\text{eff}}$  with respect to the gap, the gap equation is obtained (Sec. SIB):

$$\frac{1}{U} = F(p_s^2, |\Delta|, T) = \sum_{\mathbf{k}} \frac{f(E_{\mathbf{k}}^+) - f(E_{\mathbf{k}}^-)}{2E_{\mathbf{k}}}. \quad (\text{S3})$$

Equation (S3) has the same structure as in Fulde–Ferrell–Larkin–Ovchinnikov–type treatments with finite center-of-mass momentum [4, 9–12], and by particle-hole and angular averaging symmetries, the dependence enters as  $F(p_s^2, |\Delta|, T)$ .

Accordingly, the phase-fluctuation field  $\mathbf{p}_s = \nabla_{\mathbf{R}} \delta\theta(\mathbf{R})/2$  emerges in the SC action and gap equation here. Following discussion in Ref. [13], the phase dynamics  $\mathbf{p}_s$  can be decomposed into two orthogonal components (Helmholtz decomposition) [13]:

$$\mathbf{p}_s = \mathbf{p}_{s,\parallel} + \mathbf{p}_{s,\perp}, \quad \text{with} \quad \nabla \times \mathbf{p}_{s,\parallel} = 0 \quad \text{and} \quad \nabla \cdot \mathbf{p}_{s,\perp} = 0. \quad (\text{S4})$$

The longitudinal one  $\mathbf{p}_{s,\parallel}$  is associated with the gapless Nambu–Goldstone (NG) smooth, long-wavelength phase fluctuations and acts as the SC momentum [14–17]. Specifically, through the variation  $\delta S_{\text{eff}}$  with respect to the phase fluctuation and considering the long-wavelength approximation, one can find the equation of motion of  $\mathbf{p}_{s,\parallel}$ :

$$[\partial_t^2 + \omega_{\text{NG}}^2(q)] \mathbf{p}_{s,\parallel}(\mathbf{q}) = 0, \quad (\text{S5})$$

\* fzy5099@psu.edu

† lqc3@psu.edu

where the energy spectrum of NG mode is given by  $\omega_{\text{NG}}^2(q) = n_s q^2 / (2D_q m)$  and the superfluid density is written as (Sec. S1B)

$$n_s = 2E_F |\Delta|^2 \sum_{\mathbf{k}} \frac{\partial E_{\mathbf{k}}}{E_{\mathbf{k}}} \left[ \frac{f(E_{\mathbf{k}}^+) - f(E_{\mathbf{k}}^-)}{2E_{\mathbf{k}}} \right] \approx 2E_F |\Delta|^2 \sum_{\mathbf{k}} \frac{f(E_{\mathbf{k}}^-) - f(E_{\mathbf{k}}^+)}{2E_{\mathbf{k}}^3}. \quad (\text{S6})$$

It is noted that Eq. (S5) is exactly same as the equation of motion of the NG mode in the literature [4, 8, 14–17] and the expression of the superfluid density is also same as the one obtained in the literature by various approaches [3, 4, 6, 8, 12, 14, 18]. The statistical average of these fluctuations must be treated within quantum-statistical framework, as a consequence of the NG bosons dictated by fundamental NG theorem [15, 16, 19, 20], following the spontaneous breaking of  $U(1)$  symmetry in superconductors. From the equation of motion of NG mode, one can introduce a thermal field and then calculate the thermal phase fluctuation via the fluctuation dissipation theorem, or directly calculate the thermal phase fluctuation through the Bosonic Green function within Matsubara representation. Both approaches lead to the same results:  $\langle \mathbf{p}_{s,\parallel} \rangle = 0$  and

$$\langle p_{s,\parallel}^2 \rangle = S_{\text{th}}(T) + S_{\text{zo}}, \quad (\text{S7})$$

with the thermal-excitation part

$$S_{\text{th}}(T) = \int \frac{d\mathbf{q}}{(2\pi)^2} \frac{q^2 n_B(\omega_{\text{NG}})}{2D_q \omega_{\text{NG}}(q)}, \quad (\text{S8})$$

and the zero-point oscillation part

$$S_{\text{zo}} = \int \frac{d\mathbf{q}}{(2\pi)^2} \frac{q^2}{2D_q \omega_{\text{NG}}(q)}. \quad (\text{S9})$$

Here,  $n_B(x)$  denotes the Bose-Einstein distribution. This part enters the SC gap equation and is expected to renormalize the SC gap [4, 21–23], in a gauge manner analogous to the way a vector potential can influence the SC gap [14–16].

The transverse one  $\mathbf{p}_{s,\perp}$  encodes Berezinskii–Kosterlitz–Thouless (BKT) fluctuations, since only this part carries vorticity:

$$\pi \sum_j q_j = \oint \mathbf{p}_s \cdot d\mathbf{l} = \int_S (\nabla \times \mathbf{p}_s) \cdot ds = \int_S (\nabla \times \mathbf{p}_{s,\perp}) \cdot ds, \quad (\text{S10})$$

where  $j$  indexes individual vortices or antivortices and  $q_j \in \mathbb{Z}$  is their integer vorticity (topological charge). Equivalently,  $\nabla \times \mathbf{p}_{s,\perp} = \pi \sum_j q_j \delta(\mathbf{r} - \mathbf{r}_j)$ , a sum of point-like topological defects located at position  $\mathbf{r}_j$ . These topological defects (vortices) primarily disorder the SC phase and renormalize the superfluid stiffness, while the pairing amplitude remains essentially unchanged except within the vortex-core singularities. The BKT renormalization-group (RG) description is well established in the literature, and takes the bare superfluid density  $n_s$  as input to the standard RG equations [13, 24–27]:

$$\frac{dK}{dl} = -K^2 g^2 \quad \text{and} \quad \frac{dg}{dl} = (2 - K)g, \quad (\text{S11})$$

in which the initial conditions of the dimensionless stiffness  $K(l)$  and the vortex fugacity  $g(l)$  are given by

$$K(l=0) = \frac{\pi}{k_B T} \frac{\hbar^2 n_s}{4m} \quad \text{and} \quad g(l=0) = 2\pi e^{-\mu_v(T)/(k_B T)} \quad (\text{S12})$$

Here,  $\mu_v$  is the vortex–core energy, and following Ref. [13] for 3D superconductors, in the monolayer limit, the vortex–core energy may be estimated as the condensation energy lost inside a core of radius  $L_v$ :

$$\mu_v = \pi L_v^2 E_c \frac{n_s}{n} = \pi \frac{\hbar^2 v_F^2}{\pi^2 |\Delta|^2} \frac{D|\Delta|^2}{2} \frac{n_s}{n} = \frac{2}{\pi} \frac{\hbar^2 n_s}{4m} = \frac{2}{\pi^2} \frac{\pi \hbar^2 n_s}{4m}, \quad (\text{S13})$$

with  $L_v = \hbar v_F / (\pi |\Delta|)$  and  $E_c = D|\Delta|^2/2$  being the condensation-energy density. Thus, with Eqs. (S11)–(S13), using the bare superfluid density, integrating the BKT flow to  $l \rightarrow \infty$  yields a renormalized value  $\bar{n}_s = \frac{4m_e k_B T}{\pi \hbar^2} K(l=\infty)$ , which accounts for the vortex-antivortex fluctuations. The separatrix  $2 - \pi K = 0$  gives the Nelson–Kosterlitz universal jump [13, 24–27], while flows with  $K < 2/\pi$  run to the disordered phase (unbound vortices,  $y \rightarrow \infty$ ) and those with  $K > 2/\pi$  renormalize to a finite  $K(l=\infty)$  with  $y \rightarrow 0$  (bound vortex–antivortex pairs) [13].

Consequently, consistent with the longitudinal and transverse decomposition, only the longitudinal (curl-free) component, NG phase fluctuations, enters the SC gap equation and drives uniform pair breaking; the transverse (divergence-free) component

contributes via BKT vortex physics to the renormalization of the superfluid stiffness but does not directly modify the homogeneous amplitude equation, except for local suppression inside vortex cores.

*Disorder Modification.*—It should be emphasized that the above derivation holds in the clean limit. In practice, disorder is unavoidable in monolayer systems and affects the amplitude (gap) and phase (stiffness) sectors differently. For isotropic  $s$ -wave pairing, the SC gap equation is not renormalized by nonmagnetic impurities (Anderson theorem [28–31], Sec. SIC), whereas the superfluid density, being a current–current correlation [32, 33], is reduced by the elastic scattering, as realized by various theoretical approaches using Gorkov theory [18], Eilenberger transport [32, 34, 35], gauge-invariant kinetic equations [12], and diagrammatic formulations incorporating *vertex* corrections to the current–current correlation [32, 33]. While illuminating, such microscopic treatments are cumbersome for practical modeling to compare with experiments. Here we directly adopt Tinkham’s interpolation in the context of  $s$ -wave superconductors [36], which approximate the penetration depth  $\lambda$  as  $\lambda^2 = \lambda_{\text{clean}}^2 (1 + \xi/l)$  and hence  $n_s \rightarrow n_{s,\text{clean}} / (1 + \xi/l)$ . Thus, the superfluid-density expression [Eq. (S6)] in our framework becomes

$$\frac{n_s}{n} = \frac{1}{1 + \xi/l} \int d\xi_k \int \frac{d\theta_{\mathbf{k}}}{2\pi} \frac{|\Delta|^2}{2E_{\mathbf{k}}^3} [f(E_{\mathbf{k}}^-) - f(E_{\mathbf{k}}^+)], \quad (\text{S14})$$

where  $\xi = \hbar v_F / |\Delta|$  is the SC coherence length and  $l = v_F \gamma^{-1}$  is the mean free path, with  $\gamma$  representing the effective scattering rate, encompassing the quasiparticle decay and transport processes, and implicitly including the localization effects [1, 2, 37–41] in the disordered regime. This prescription is consistent with the Mattis–Bardeen dirty-limit result [6, 42] and Nam’s extension to arbitrary scattering strength [43], and has been shown to successfully account for early experimental measurements of the penetration depth  $\lambda$  [44–47].

In the following, we present the detailed length derivations.

### A. Derivation of effective action

From the Hamiltonian (S1), the action of this model is given by [4–8]

$$S[\psi, \psi^\dagger] = \int dx \left\{ \sum_s \psi_s^\dagger(x) (i\partial_{x_0} - \xi_{\hat{\mathbf{p}}}) \psi_s(x) + U \psi_\uparrow^\dagger(x) \psi_\downarrow^\dagger(x) \psi_\downarrow(x) \psi_\uparrow(x) \right\} - \frac{1}{2} \sum_{ss'} \int dx dx' V(x - x') \psi_s^\dagger(x) \psi_{s'}^\dagger(x') \psi_{s'}(x') \psi_s(x), \quad (\text{S15})$$

where the four-vector  $x = (x_0, \mathbf{x})$ . Applying the Hubbard-Stratonovich transformation [4–8], one has

$$S[\psi, \psi^\dagger] = \sum_s \int dx \psi_s^\dagger(x) [i\partial_{x_0} - \xi_{\hat{\mathbf{p}}} - \mu_H(x)] \psi_s(x) - \int dx \left[ \psi^\dagger(x) \hat{\Delta}(x) \psi(x) + \frac{|\Delta(x)|^2}{U} \right] + \frac{1}{2} \int dx_0 d\mathbf{q} \frac{|\mu_H(x_0, \mathbf{q})|^2}{V_{\mathbf{q}}}. \quad (\text{S16})$$

Here,  $\psi(x) = [\psi_\uparrow(x), \psi_\downarrow^\dagger(x)]^T$  represents the field operator in Nambu space;  $\hat{\Delta}(x) = \Delta(x)\tau_+ + \Delta^*(x)\tau_-$  with  $\tau_i$  being the Pauli matrices in Nambu space [18]; the SC order parameter  $\Delta(x) = |\Delta(x)|e^{i\delta\theta(x)}$  with  $|\Delta(x)|$  and  $\delta\theta(x)$  being the SC gap and phase, respectively;  $\mu_H(x_0, \mathbf{q})$  stands for the Hartree field.

Using the unitary transformation  $\psi(x) \rightarrow e^{i\tau_3 \delta\theta(x)/2} \psi(x)$  to effectively remove the SC phase from the order parameter, the above action becomes

$$S = \int dx \left\{ \sum_s \psi_s^\dagger(x) \left[ i\partial_{x_0} - \frac{\partial_{x_0} \delta\theta(x)}{2} - \xi_{\hat{\mathbf{p}} + \mathbf{p}_s} - \mu_H(x) \right] \psi_s(x) - \psi^\dagger(x) |\Delta(x)| \tau_1 \psi(x) - \frac{|\Delta(x)|^2}{U} \right\} + \int dx_0 d\mathbf{q} \frac{|\mu_H(x_0, \mathbf{q})|^2}{2V_{\mathbf{q}}}, \quad (\text{S17})$$

where the phase fluctuations  $\mathbf{p}_s = \nabla \delta\theta / 2$ .

By separating center-of-mass [ $R = \frac{x_1 + x_2}{2} = (t, \mathbf{R})$ ] and relative [ $r = x_1 - x_2 = (\tau, \mathbf{r})$ ] coordinates of the pairing electrons [3–8, 18], within the assumption of a macroscopically homogeneous gap and  $\xi_{\hat{\mathbf{p}} + \mathbf{p}_s} = \xi_{\hat{\mathbf{k}}} + \mathbf{p}_s \cdot \mathbf{v}_{\hat{\mathbf{k}}} + \mathbf{p}_s^2 / (2m)$ , one obtains

$$\begin{aligned} S[\psi, \psi^\dagger] &= \int dx \psi^\dagger(x) \left\{ (i\partial_\tau - \mathbf{p}_s \cdot \mathbf{v}_{\hat{\mathbf{k}}} - \xi_{\hat{\mathbf{k}}} \tau_3 - |\Delta| \tau_1) + \left[ \frac{p_s^2}{2m} + \mu_H(R) + \frac{\partial_t \delta\theta(R)}{2} \right] \tau_3 \right\} \psi(x) \\ &\quad - \int dR \left( \frac{p_s^2}{2m} + \frac{|\Delta|^2}{U} + \mu_H(R) + \frac{\partial_t \delta\theta(R)}{2} \right) + \frac{1}{2} \int dt d\mathbf{q} \frac{|\mu_H(\mathbf{q}, x_0)|^2}{V_{\mathbf{q}}} \\ &= \int dx \psi^\dagger(x) \left\{ (i\partial_\tau - \mathbf{p}_s \cdot \mathbf{v}_{\hat{\mathbf{k}}} - \xi_{\hat{\mathbf{k}}} \tau_3 - |\Delta| \tau_1) + \left[ \frac{p_s^2}{2m} + \mu_H(R) + \frac{\partial_t \delta\theta(R)}{2} \right] \tau_3 \right\} \psi(x) \\ &\quad - \int dR \left( \frac{p_s^2}{2m} + \frac{|\Delta|^2}{U} \right) + \frac{1}{2} \int dt d\mathbf{q} \frac{|\mu_H(\mathbf{q}, x_0)|^2}{V_{\mathbf{q}}}. \end{aligned} \quad (\text{S18})$$

Then, through the standard integration over the Fermi field [4–8], one has

$$S = \int dR \left( \bar{\text{Tr}} \ln G_0^{-1} - \sum_n^{\infty} \frac{1}{n} \bar{\text{Tr}} \{ [\Sigma(R) G_0]^n \} \right) - \int dR \left( \frac{p_s^2}{2m} + \frac{|\Delta|^2}{U} \right) + \frac{1}{2} \int dt d\mathbf{q} \frac{|\mu_H(\mathbf{q}, x_0)|^2}{V_q}, \quad (\text{S19})$$

where the Green function in the Matsubara representation and momentum space:

$$G_0(p) = \frac{i p_n \tau_0 - \mathbf{p}_s \cdot \mathbf{v}_k \tau_0 + \xi_k \tau_3 + |\Delta| \tau_1}{(i p_n - E_k^+)(i p_n - E_k^-)}, \quad (\text{S20})$$

and self-energy:

$$\Sigma = \left[ \frac{p_s^2}{2m} + \mu_H(R) + \frac{\partial_t \delta \theta(R)}{2} \right] \tau_3. \quad (\text{S21})$$

Here, the four-vector  $p = (i p_n, \mathbf{k})$ . Keeping the lowest two orders (i.e.,  $n = 1$  and  $n = 2$ ) leads to the result:

$$S = \int dR \left\{ \sum_{p_n, \mathbf{k}} \ln[(i p_n - E_k^+)(i p_n - E_k^-)] - \tilde{\chi}_3 \frac{p_s^2}{2m} + \chi_{33} \left[ \frac{p_s^2}{2m} + \mu_H(R) + \frac{\partial_t \delta \theta(R)}{2} \right]^2 - \frac{|\Delta|^2}{U} \right\} + \frac{1}{2} \int dt d\mathbf{q} \frac{|\mu_H(\mathbf{q}, x_0)|^2}{V_q}, \quad (\text{S22})$$

where the correlation coefficients are given by

$$\tilde{\chi}_3 = \sum_{\mathbf{k}} \left[ 1 + \sum_{p_n} \text{Tr}[G_0(p) \tau_3] \right] = \sum_{\mathbf{k}} \left[ 1 + \frac{\xi_k}{E_k} (f(E_k^+) - f(E_k^-)) \right] = -\frac{k_F^2}{2m} \sum_{\mathbf{k}} \partial_{\xi_k} \left[ \frac{\xi_k}{E_k} (f(E_k^+) - f(E_k^-)) \right] = n, \quad (\text{S23})$$

$$\chi_{33} = -\frac{1}{2} \sum_p \text{Tr}[G_0(p) \tau_3 G_0(p) \tau_3] = -\sum_{p_n, \mathbf{k}} \frac{(i p_n - \mathbf{p}_s \cdot \mathbf{v}_k)^2 + \xi_k^2 - |\Delta|^2}{(i p_n - E_k^+)^2 (i p_n - E_k^-)^2} = -\sum_{\mathbf{k}} \partial_{\xi_k} \left[ \frac{\xi_k}{2E_k} (f(E_k^+) - f(E_k^-)) \right] = D. \quad (\text{S24})$$

Further through the integration over the Hartree field, one finally arrives at the effective action of the gap and phase fluctuation:

$$S_{\text{eff}} = \int dR \left\{ \sum_{p_n, \mathbf{k}} \ln[(i p_n - E_k^+)(i p_n - E_k^-)] - \frac{n p_s^2}{2m} - \frac{|\Delta|^2}{U} \right\} + \int dt d\mathbf{q} \frac{D}{1 + 2D V_q} \left( \frac{\partial_t \delta \theta(\mathbf{q})}{2} + \frac{p_s^2}{2m} \right)^2, \quad (\text{S25})$$

which gives rise to Eq. (S2) by neglecting the high-order mutual interaction between phase fluctuations.

## B. Derivation of thermodynamic equations

Through the Euler-Lagrange equation of motion with respect to the SC gap, i.e.,  $\partial_{|\Delta|} S_{\text{eff}} = 0$ , one has

$$0 = \frac{|\Delta|}{U} + \sum_{p_n, \mathbf{k}} \frac{|\Delta|}{(i p_n - E_k^+)(i p_n - E_k^-)} = \frac{|\Delta|}{U} + \sum_{\mathbf{k}} \frac{|\Delta|}{2E_k} [f(E_k^+) - f(E_k^-)]. \quad (\text{S26})$$

Through the Euler-Lagrange equation of motion with respect to the long-wavelength phase fluctuation, i.e.,  $\partial_{\mu} \left[ \frac{\partial S_{\text{eff}}}{\partial (\partial_{\mu} \delta \theta / 2)} \right] = \partial_{\delta \theta / 2} S_{\text{eff}}$ , in frequency and momentum space, the equation of motion of the NG phase fluctuations reads

$$\left( \frac{n_s q^2}{2m} - D_q \omega^2 \right) \frac{\delta \theta(\omega, \mathbf{q})}{2} = 0, \quad (\text{S27})$$

where the superfluid density is determined by

$$\begin{aligned} \frac{n_s \mathbf{p}_s}{m} &= \frac{n \mathbf{p}_s}{m} + \sum_{p_n, \mathbf{k}} \frac{2\mathbf{k}(i p_n - \mathbf{k} \cdot \mathbf{p}_s / m)}{m(i p_n - E_k^+)(i p_n - E_k^-)} = \frac{\mathbf{p}_s k_F^2}{m^2} \sum_{\mathbf{k}} \left\{ -\partial_{\xi_k} \left[ \frac{\xi_k}{2E_k} (f(E_k^+) - f(E_k^-)) \right] + \partial_{E_k} \left[ \frac{f(E_k^+) - f(E_k^-)}{2} \right] \right\} \\ &= \frac{\mathbf{p}_s}{m} \frac{k_F^2}{m} \sum_{\mathbf{k}} \frac{|\Delta|^2}{E_k} \partial_{E_k} \left[ \frac{f(E_k^+) - f(E_k^-)}{2E_k} \right]. \end{aligned} \quad (\text{S28})$$

Equation (S27) is exactly same as the equation of motion of the NG mode in the literature [4, 8, 14–17], and substituting  $\mathbf{p}_s(\mathbf{q}) = i\mathbf{q}\delta\theta(\mathbf{q})/2$  leads to Eq. (S5).

From the equation of motion of the NG phase fluctuation, one can derive the thermal phase fluctuation through the fluctuation dissipation theorem or within Matsubara formalism. The two methods are equivalent, and lead to the exactly same result.

*Fluctuation dissipation theorem.*—Considering the thermal fluctuation, the dynamics of the phase from Eq. (S27) is given by

$$\left( \frac{n_s q^2}{2m} - D_q \omega^2 + i\omega\gamma \right) \frac{\delta\theta(\omega, \mathbf{q})}{2} = J_{\text{th}}(\omega, \mathbf{q}). \quad (\text{S29})$$

Here, we have introduced a thermal field  $\mathbf{J}_{\text{th}}(\omega, \mathbf{q})$  that obeys the fluctuation-dissipation theorem [48]:

$$\langle J_{\text{th}}(\omega, \mathbf{q}) J_{\text{th}}^*(\omega', \mathbf{q}') \rangle = \frac{(2\pi)^3 \gamma \omega \delta(\omega - \omega') \delta(\mathbf{q} - \mathbf{q}')}{\tanh(\beta\omega/2)}, \quad (\text{S30})$$

and  $\gamma = 0^+$  is a phenomenological damping constant. From this dynamics, the average of the phase fluctuations is given by

$$\begin{aligned} \langle p_{s,\parallel}^2 \rangle &= \int \frac{d\omega d\omega' d\mathbf{q} d\mathbf{q}'}{(2\pi)^6} \frac{(\mathbf{q} \cdot \mathbf{q}') \langle J_{\text{th}}(\omega, \mathbf{q}) J_{\text{th}}^*(\omega', \mathbf{q}') \rangle}{[D_q(\omega^2 - \omega_{\text{NG}}^2(\mathbf{q})) - i\omega\gamma][D_{q'}(\omega'^2 - \omega_{\text{NG}}^2(\mathbf{q}')) + i\omega'\gamma]} = \int \frac{d\omega d\mathbf{q}}{(2\pi)^3} \frac{q^2 \gamma \omega / \tanh(\beta\omega/2)}{[D_q(\omega^2 - \omega_{\text{NG}}^2(\mathbf{q}))]^2 + \omega^2 \gamma^2} \\ &= \int \frac{d\mathbf{q}}{(2\pi)^2} \frac{q^2}{2D_q \omega_{\text{NG}}(q)} [2n_B(\omega_{\text{NG}}) + 1]. \end{aligned} \quad (\text{S31})$$

*Matsubara formalism.*—Within the Matsubara formalism, by mapping into the imaginary-time space, from Eq. (S27), the thermal phase fluctuation reads [18]

$$\begin{aligned} \langle p_{s,\parallel}^2 \rangle &= \int \frac{d\mathbf{q}}{(2\pi)^2} q^2 \left[ \left\langle \left| \frac{\delta\theta^*(\tau, \mathbf{q})}{2} \frac{\delta\theta(\tau, \mathbf{q})}{2} e^{-\int_0^\beta d\tau d\mathbf{q} D_q \delta\theta^*(\tau, \mathbf{q})(\omega_{\text{NG}}^2 - \partial_\tau^2) \delta\theta(\tau, \mathbf{q})/4} \right| \right\rangle \right] \\ &= \int \frac{d\mathbf{q}}{(2\pi)^2} q^2 \left[ \frac{1}{Z_0} \int D\delta\theta D\delta\theta^* \frac{\delta\theta^*(\tau, \mathbf{q})}{2} \frac{\delta\theta(\tau, \mathbf{q})}{2} e^{-\int_0^\beta d\tau d\mathbf{q} D_q \delta\theta^*(\tau, \mathbf{q})(\omega_{\text{NG}}^2 - \partial_\tau^2) \delta\theta(\tau, \mathbf{q})/4} \right] \\ &= \int \frac{d\mathbf{q}}{(2\pi)^2} q^2 \frac{1}{Z_0} \int D\delta\theta D\delta\theta^* \delta_{J_q^*} \delta_{J_q} e^{-\int_0^\beta d\tau d\mathbf{q} [D_q \delta\theta^*(\tau, \mathbf{q})(\omega_{\text{NG}}^2 - \partial_\tau^2) \delta\theta(\tau, \mathbf{q})/4 + J_q \delta\theta(\mathbf{q})/2 + J_q^* \delta\theta^*(\mathbf{q})/2]} \Big|_{J=J^*=0} \\ &= \int \frac{d\mathbf{q}}{(2\pi)^2} \frac{q^2}{D_q} \delta_{J_q^*} \delta_{J_q} \exp \left\{ - \int_0^\beta d\tau \sum_{\mathbf{q}'} J_{\mathbf{q}'} \frac{1}{\partial_\tau^2 - \omega_{\text{NG}}^2} J_{\mathbf{q}'}^* \right\} \Big|_{J=J^*=0} = - \int \frac{d\mathbf{q}}{(2\pi)^2} \frac{1}{\beta} \sum_{\omega_n} \frac{q^2}{D_q} \frac{1}{(i\omega_n)^2 - \omega_{\text{NG}}^2} \\ &= \int \frac{d\mathbf{q}}{(2\pi)^2} \frac{q^2}{2D_q \omega_{\text{NG}}(q)} [2n_B(\omega_{\text{NG}}) + 1], \end{aligned} \quad (\text{S32})$$

which is exactly the same as the one in Eq. (S31) obtained via fluctuation dissipation theorem. Here,  $\omega_n = 2n\pi T$  represents the Bosonic Matsubara frequencies;  $J_{\mathbf{q}}$  denotes the generating functional and  $\delta J_{\mathbf{q}}$  stands for the functional derivative.

The fundamental derivation of BKT fluctuations and the corresponding RG equations has been well established in the literature and will not be repeated here.

### C. Anderson theorem

To facilitate the reading and understanding of the texts and supplementary materials, we reproduce here the well-known the Anderson theorem [28–31]. We start with the Gorkov equation in Matsubara presentation:

$$[ip_n - H_0(\mathbf{k}) - \Sigma(ip_n, \mathbf{k})]G(ip_n, \mathbf{k}) = 1, \quad (\text{S33})$$

where the Bogoliubov–de Gennes Hamiltonian  $H_0(\mathbf{k}) = \xi_{\mathbf{k}}\tau_3 + \Delta_0\tau_1$  and the self-energy of the electron-impurity interaction  $V_{\mathbf{kk}'}$  reads[30]

$$\Sigma(ip_n, \mathbf{k}) = c_i \sum_{\mathbf{k}'} V_{\mathbf{kk}'} \tau_3 G(ip_n, \mathbf{k}') \tau_3 V_{\mathbf{k}'\mathbf{k}}. \quad (\text{S34})$$

Without the disorder, the bare Green function of the conventional BCS superconductors is established as

$$G_0(ip_n, \mathbf{k}) = \frac{ip_n + \xi_{\mathbf{k}}\tau_3 + \Delta_0\tau_1}{(ip_n)^2 - \xi_{\mathbf{k}}^2 - \Delta_0^2}. \quad (\text{S35})$$

With the disorder, to self-consistently calculate the Green function from Eq. (S33), one can consider a renormalized equation as [28–31]

$$ip_n - H_0(k) - \Sigma(ip_n, \mathbf{k}) = i\tilde{p}_n - \tilde{H}_0(k) = i\tilde{p}_n - \xi_{\mathbf{k}}\tau_3 - \tilde{\Delta}_0\tau_1, \quad (\text{S36})$$

which leads to the Green function

$$G(ip_n, k) = \frac{i\tilde{p}_n\tau_0 + \xi_{\mathbf{k}}\tau_3 + \tilde{\Delta}_0\tau_1}{(i\tilde{p}_n)^2 - \xi_{\mathbf{k}}^2 - \tilde{\Delta}_0^2}. \quad (\text{S37})$$

Substituting Eq. (S37) to Eq. (S36), one has

$$\tilde{p}_n = p_n + \Gamma_0 \frac{\tilde{p}_n}{\sqrt{(\tilde{p}_n)^2 + \Delta_0^2}}, \quad (\text{S38})$$

$$\tilde{\Delta}_0 = \Delta_0 + \Gamma_0 \frac{\tilde{\Delta}_0}{\sqrt{(\tilde{p}_n)^2 + \Delta_0^2}}, \quad (\text{S39})$$

where  $\Gamma_0 = c_i \pi N(0) \int d\Omega_{\mathbf{k}'} |V_{\mathbf{k}\mathbf{k}'}|^2$ . From equations above, it can be demonstrated that  $p_n/\Delta_0 = \tilde{p}_n/\tilde{\Delta}_0$ .

Consequently, from the gap equation  $\Delta_0 = -gT \sum_{n,\mathbf{k}} \text{Tr}[G(ip_n, \mathbf{k})\tau_1/2]$ , one finds

$$\Delta_0 = gT \sum_n \int d\mathbf{k} \frac{\tilde{\Delta}_0}{\xi_{\mathbf{k}}^2 + \tilde{\Delta}_0^2 + (\tilde{p}_n)^2} = \sum_n \frac{gTN(0)\pi}{\sqrt{1 + (\tilde{p}_n/\tilde{\Delta}_0)^2}} = \sum_n \frac{gTN(0)\pi}{\sqrt{1 + (p_n/\Delta_0)^2}}, \quad (\text{S40})$$

which is exactly same as the one without the disorder. This indicates that the SC gap equation is insensitive to the non-magnetic impurities, i.e., the SC gap equation experiences a null renormalization by non-magnetic impurities [28–31].

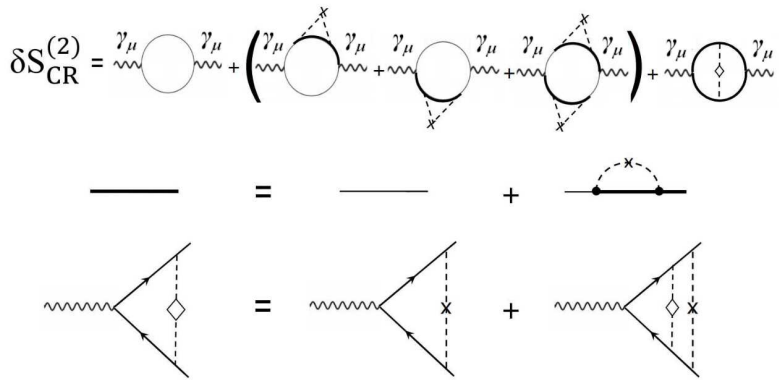


FIG. SI. Diagrammatic formalism for the current-current correlation. The first diagram on the right-hand side of  $\delta S_{\text{CR}}^{(2)}$  denotes the bare current-current correlation, while the second and third diagrams represent the Born and vertex corrections due to impurity scattering, respectively. Dashed lines with a cross and a diamond denote the impurity potential and the ladder-type series of impurity scatterings. The wavy line corresponds to the external field, and  $\gamma_{\mu}$  represents the vertex function, i.e., the four-vector current  $\gamma_{\mu} = [\tau_3, \hat{\mathbf{k}}/m]$  [5, 16, 43]. Thin solid lines denote the bare SC Green's functions, while thick solid lines denote the impurity-renormalized SC Green's functions.

In contrast, the calculation of the superfluid density arises from the current-current correlation function, where vertex corrections due to impurity scattering necessarily appear (Fig. SI). These corrections vanish in the equilibrium case but become essential for evaluating dynamical or fluctuating responses. Consequently, the superfluid density is renormalized by disorder, in sharp contrast to the robustness of the SC gap. This can be directly seen from the Mattis-Bardeen formula in the dirty limit, where the penetration depth (or equivalently the superfluid stiffness) depends explicitly on the scattering rate through [36, 42]

$$1/\lambda^2(0) \propto |\Delta_0| \sigma_n, \quad \sigma_n = ne^2\tau/m, \quad (\text{S41})$$

or equivalently

$$\frac{n_s(T=0)}{n} \propto \frac{l}{\xi} \quad (\text{dirty limit}). \quad (\text{S42})$$

Here,  $\sigma_n$  represents the electrical conductivity in normal metals with  $\tau$  being the the momentum-relaxation time. Clearly, while the gap  $|\Delta_0|$  remains insensitive to nonmagnetic impurities, the factor  $\sigma_n \propto \tau$  carries the dependence on the quasiparticle scattering time  $\tau$ , demonstrating how disorder suppresses the superfluid density without affecting the gap amplitude.

A fully rigorous treatment would require a microscopic analysis of scattering processes by various theoretical approaches using Gorkov theory [18], Eilenberger transport [32, 34, 35], gauge-invariant kinetic equations [12], and diagrammatic formulations incorporating *vertex* corrections to the current-current correlation [32, 33], which we do not repeat here.

## SII. Simulation treatment

In the specific simulation, a subtle point arises regarding the treatment of the zero-point oscillations of the bosonic NG-mode excitations in Eq. (S7). If not handled properly, this contribution can violate fundamental principles. For instance, in the absence of disorder, the finite expectation value  $\langle p_{s,\parallel}^2 \rangle$  generated by the zero-point term  $S_{\text{zo}}$  in Eq. (S7) would imply a reduced superfluid density  $n_s(T = 0) < n$  in Eq. (S6), in contradiction with Galilean invariance. As discussed in Refs. [49, 50], this inconsistency for superfluid density can be resolved by introducing a shift of the chemical potential.

In practice, this issue related to the bosonic excitation is not unique to superconductivity but is also known in the *ab initio* calculations of lattice vibrations within density functional theory. There, the effect of zero-point oscillations is typically absorbed into the renormalized model parameters [51, 52], so that subsequent phonon excitations are described solely by the Bose distribution  $n_B(x)$ . This approach is consistent with the general field-theoretical treatment of zero-point oscillations [53], where the vacuum is not strictly empty but is continuously populated by zero-point fluctuating excitations. In doing so, the treatment enforces both the Ward identity and the *f*-sum rule, and is essentially equivalent to field-theoretical normal ordering [53], in which the vacuum-related, temperature-independent contribution is absorbed into the ground-state parameters. Such a procedure has proven effective in the study of lattice dynamics, particularly in quantum paraelectrics [51, 52, 54–56]. We thus adopt the same strategy here. Concretely, we subtract the zero-point contribution  $S_{\text{zo}}$  in the phase-fluctuation generation of Eq. (S6) by incorporating it into the pairing potential, i.e., by renormalizing  $U$  to  $\tilde{U}$ . The quantities  $\tilde{U}$  and  $\langle p_{s,\parallel}^2 \rangle = S_{\text{th}}$  then replace  $U$  and  $\langle p_{s,\parallel}^2 \rangle = S_{\text{th}} + S_{\text{zo}}$  in the framework, respectively. The renormalized pairing potential is defined as

$$\frac{1}{\tilde{U}} = F[p_{s,\parallel}^2 = 0, |\Delta(T = 0)|, T = 0], \quad (\text{S43})$$

whereas  $|\Delta(T = 0)|$  is self-consistently determined from the original gap equation including the zero-point oscillation,

$$\frac{1}{U} = F[p_{s,\parallel}^2 = S_{\text{zo}}, |\Delta(T = 0)|, T = 0]. \quad (\text{S44})$$

This construction guarantees that the zero-point renormalization of the gap remains unchanged, in consistency with the previous studies [4, 21–23] and, in particular, that the superfluid density satisfies  $n_s(T = 0) = n$  in the clean limit, in consistency with Galilean invariance and previous studies [49, 50]. Importantly, this procedure disentangles the zero-point contribution from genuine thermal fluctuations. The former is absorbed into the renormalized pairing interaction at  $T = 0$ , whereas the latter,

$$\frac{1}{\tilde{U}} = F[p_{s,\parallel}^2 = S_{\text{th}}(T, n_s(T)), |\Delta(T)|, T], \quad (\text{S45})$$

exclusively govern the finite-temperature phase-fluctuation physics, as is physically required. It should be emphasized that within this procedure, all physical quantities at  $T = 0$  and in the  $T = 0^+$  limit are mathematically continuous and mutually self-consistent.

Thus, for each doping level (Fermi energy) and disorder strength, our simulation proceeds in two steps. First, we self-consistently solve the zero-temperature gap equation [Eq. (S44)], the zero-point NG phase fluctuations [Eq. (S9)], and the disorder-modified superfluid density [Eq. (S14)] using an iterative procedure, thereby obtaining the zero-point-renormalized gap and hence the pairing potential [Eq. (S43)]. Next, we solve the finite-temperature gap equation [Eq. (S45)], the thermal NG phase fluctuations [Eq. (S8)], and the disorder-modified superfluid density [Eq. (S14)] in the same iterative manner. Substituting the resulting bare finite-temperature superfluid density into the BKT renormalization-group equations [Eqs. (S11)–(S13)] then allows us to determine the full set of SC properties. The SC transition temperature  $T_c$  is determined from the condition  $\bar{n}_s(T_c) = 0$  while the gap-closing temperature  $T_{\text{os}}$  is obtained by  $|\Delta(T = T_{\text{os}})| = 0$ .

The electron density  $n_e = 2n$  (reflecting the twofold valley degeneracy at  $\pm Q$ ) and the hole density  $n_h$  are determined by the Fermi energy  $E_F$  and the negative band gap  $E_g$  within the parabolic-band 2DEG approximation:  $n = 2DE_F$  with the electron density of states  $D = m_e/(2\pi\hbar^2)$  and  $n_h = 2m_h/(2\pi\hbar^2) \times (|E_g| - E_F)\theta(|E_g| - E_F)$ . The energy zero is chosen at the conduction-band minimum; in the pristine case, the Fermi level thus coincides with the conduction-band edge, consistent with experimental observations showing that monolayer WTe<sub>2</sub> is effectively *p*-type at zero gate bias.

Moreover, as discussed in the main text, to approximately model the competition with the excitonic insulator phase (which in monolayer WTe<sub>2</sub> is sufficiently strong to dominate over the electron SC channel [57–61]), we assume that each hole binds

with one conduction electron to form an exciton, thereby depleting the electrons available for SC pairing. This procedure is implemented specifically by reducing the effective density of states entering the electron-SC gap equation and the superfluid density by a factor of  $(n_e - n_h)/n_e$  in the self-consistent numerical simulation.

TABLE SI. Parameters used in simulation. The electron and hole effective masses in monolayer WTe<sub>2</sub> are obtained from our DFT calculations (Sec. SIII),  $m_e \approx 0.33m_0$  and  $m_h \approx 0.53m_0$ . The pairing potential and the energy range of the attractive interaction are not available in the literature. Given that the experimentally observed SC transition temperatures largely lie below 1 K, we restrict our analysis to the vicinity of the Fermi surface within an energy cutoff of  $E_c \sim 2$  K. The pairing potential  $U$  relevant to the experiments in Refs. [58–61] is determined by fitting the SC transition temperature in the high-density regime (mean-field regime). The momentum cutoff  $q_{\text{cutoff}}$  in the bosonic integrals of the NG-mode excitation is chosen as  $1/\xi$ , in consistency with the previous studies [4, 21, 22], and this is because that the quasiparticle scattering processes effectively limit the phase coherence at length scales shorter than the SC coherence length. As a result, NG phase fluctuations with wavelengths shorter than the SC coherence length are strongly suppressed and do not contribute appreciably to the thermodynamic dynamics. It should also be emphasized that the effective scattering time  $1/\gamma$  considered here, in principle, reflects all scattering processes (corresponding approximately to the quantum lifetime), rather than only the momentum-relaxation time inferred from the mobility.

Simulation parameters used in the main text	Fig. 1	Figs. 2(b), inset and Fig. 3	Fig. 2(c)	inset of Fig. 2(c)	Fig. 2(d)
$DU/2$	0.462	0.554	0.40	0.423	0.506
$ E_g $ (meV)	0	39	26	29	18
$\gamma$ (meV)	0.4	3.5	0.8	0.54	0.07
Corresponding experiments	–	Ref. [60]	Ref. [58]	Ref. [59]	Ref. [61]

### SIII. Density-functional-theory calculation

The first-principles density functional theory simulations are performed with projector augmented-wave method implemented in the Vienna ab initio Simulation Package (VASP) [62, 63]. The exchange-correlation functional is the Perdew–Burke–Ernzerhof (PBE) type generalized gradient approximation (GGA) [64]. The plane wave cutoff energy is set as 600 eV. For the full atomic relaxation with a fixed vacuum layer larger than 20 Å and free in-plane lattice parameters, we included the DFT-D3 Van der Waals correction with Becke-Johnson damping [65], following the same settings as in our previous work [66]. The relaxation is converged after all the atomic forces are below 1 meV/Å, and electronic energy convergence criterion was set to  $1 \times 10^{-7}$  eV. We used a  $\Gamma$ -centered k-point grid of  $9 \times 5 \times 1$  for relaxation and  $20 \times 10 \times 1$  for static electronic calculations. We considered 14 valence electrons for the W element and 6 for the Te element. The relaxed in-plane lattice parameters are 3.453 and 6.262 Å, respectively. Spin-orbit coupling (SOC) is considered for static and band structure calculations to account for the band inversion.

Electron and hole effective masses are extracted from parabolic fitting of the band dispersion  $E(k)$  around the conduction band minimum and valence band maximum, respectively. Both the x- and y-direction effective masses were evaluated, from additional k-lines sampled crossing the corresponding extreme points along orthogonal directions, as shown in Table SII. These results indicate nearly isotropic electron effective masses, and lightly anisotropic hole effective masses, where the relatively higher hole effective mass along the x-direction (zigzag) is consistent with the experimental result in Ref. [67].

TABLE SII. Effective masses of electrons and holes obtained from quadratic fits of band dispersions near the conduction band minimum (CBM) and valence band maximum (VBM) along the x- and y-directions. The quality of the fits is characterized by the coefficient of determination  $R^2$ , with  $R^2 \approx 1$  indicating high reliability.

Range k-range (Å <sup>-1</sup> )	CBM-x				CBM-y				VBM-x				VBM-y			
	k-points	$m^*/m_0$	$\Delta E$ (eV)	$R^2$												
[-0.020,+0.020]	19	0.324	0.0043	0.965	0.336	0.0042	0.959	0.549	0.0025	0.960	0.516	0.0027	0.960	0.516	0.0027	0.960
[-0.030,+0.030]	29	0.321	0.0107	0.971	0.333	0.0098	0.982	0.552	0.0059	0.983	0.517	0.0063	0.982	0.517	0.0063	0.982
[-0.040,+0.040]	39	0.314	0.0206	0.965	0.329	0.0181	0.990	0.557	0.0105	0.990	0.518	0.0114	0.990	0.518	0.0114	0.990
[-0.050,+0.050]	49	0.305	0.0355	0.949	0.325	0.0290	0.993	0.564	0.0163	0.994	0.520	0.0179	0.994	0.520	0.0179	0.994

#### SIV. Potential of hole-SC state

In this part, we construct a toy model to examine the possibility of the hole-SC state on the electron-doped side. Specifically, the total hole density is given by

$$n_h = 2D_h(E_g - E_F)\theta(E_g - E_F), \quad (\text{S46})$$

where  $D_h = m_h/(2\pi\hbar^2)$  is the density of states of the hole band,  $\theta(x)$  is the step function, and  $E_g$  is the band gap at which holes begin to emerge. We assume that excitonic pairing sets in only once the hole density exceeds a certain threshold  $n_h^*$ , beyond which the excitonic phase rapidly preempts the hole-SC state. In the strong-disorder regime, the SC gap of the holes is directly suppressed due to their small phase stiffness, as discussed in the main text, so that  $n_h^* = 0$ , i.e., any finite hole density immediately participates in excitonic pairing. Under weak disorder, however, we can assume  $n_h^* > 0$ , and beyond this point, the hole-sector SC state is rapidly quenched as the excitonic phase preempts it. In this case, within the SC framework in the main text, by incorporating the effective hole mass ( $m_h \approx 0.53m_0$ ) obtained from our DFT calculations and tuning  $E_g$ ,  $n_h^*$ , the SC pairing potential of the holes and the corresponding disorder strength (weak disorder), we can reproduce the dome-like evolution of the additional SC channel, which closely resembles the experimental observations in a quantitative manner, as shown in Fig. SII.

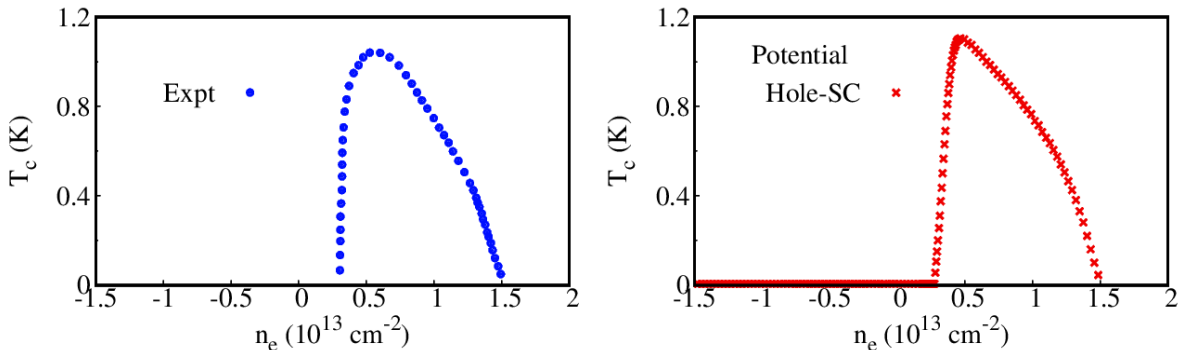


FIG. SII. Possibility of hole superconductivity on the electron-doping side. In the figure, the density  $n_e = 4DE_F$  with the electron density of states  $D = m_e/(2\pi\hbar^2)$ . Blue circles in left panel are extracted from the experimentally observed  $T_c$  of the superconductivity that survives at  $H = 50$  mT [61]. Red crosses in right panel show the calculated  $T_c$  from our toy model. In the simulation,  $D_h U_h/2 = 0.703$  with  $U_h$  being the pairing potential of hole-SC state.  $\gamma = 0.36$  meV,  $E_g = 55$  meV and  $n_h^* = 0.66 \times 10^{13}/\text{cm}^2$ .

We emphasize, however, that this model is merely an illustrative construct intended solely to visualize a plausible scenario of the hole-SC channel on the electron-doping side, and is included only for heuristic completeness. It offers no conceptual or meaningful advance, as the hole-SC channel depicted here could also be replaced by other unconventional pairing channel without loss of generality. A fully rigorous microscopic analysis would require additional experimental constraints, such as scanning tunneling microscopy (STM) measurements of the SC gap(s) or independent evidence for multiband superconductivity, as well as *ab initio* estimates of the pairing interactions in both the conduction and valence bands. These inputs are essential to clarify the competition, possible coexistence, and mutual coupling among the three candidate many-body states on the electron-doping side: electron-SC, hole-SC, and excitonic-insulator phases, but beyond the scope of the present study.

---

[1] Z.-X. Li, S. A. Kivelson, and D.-H. Lee, Superconductor-to-metal transition in overdoped cuprates, *npj Quantum Mater.* **6**, 36 (2021).  
[2] Y. Dubi, Y. Meir, and Y. Avishai, Nature of the superconductor-insulator transition in disordered superconductors, *Nature* **449**, 876 (2007).  
[3] F. Yang and M. Wu, Gauge-invariant microscopic kinetic theory of superconductivity: Application to the optical response of Nambu-Goldstone and Higgs modes, *Phys. Rev. B* **100**, 104513 (2019).  
[4] F. Yang and M. Wu, Theory of coupled dual dynamics of macroscopic phase coherence and microscopic electronic fluids: Effect of dephasing on cuprate superconductivity, *Phys. Rev. B* **104**, 214510 (2021).  
[5] J. Schrieffer, *Theory of Superconductivity* (W.A. Benjamin, 1964).  
[6] F. Yang and M. Wu, Diamagnetic property and optical absorption of conventional superconductors with magnetic impurities in linear response, *Phys. Rev. B* **109**, 064508 (2024).

- [7] F. Yang and M. Wu, Optical response of higgs mode in superconductors at clean limit, *Ann. Phys.* **453**, 169312 (2023).
- [8] Z. Sun, M. Fogler, D. Basov, and A. J. Millis, Collective modes and terahertz near-field response of superconductors, *Phys. Rev. Res.* **2**, 023413 (2020).
- [9] P. Fulde and R. A. Ferrell, Superconductivity in a strong spin-exchange field, *Phys. Rev.* **135**, A550 (1964).
- [10] A. Larkin and Y. N. Ovchinnikov, Nonuniform state of superconductors, *JETP* **20**, 762 (1965).
- [11] F. Yang and M. W. Wu, Fulde–Ferrell state in spin–orbit-coupled superconductor: Application to Dresselhaus SOC, *J. Low Temp. Phys.* **192**, 241 (2018).
- [12] F. Yang and M. Wu, Gauge-invariant microscopic kinetic theory of superconductivity in response to electromagnetic fields, *Phys. Rev. B* **98**, 094507 (2018).
- [13] L. Benfatto, *The Berezinskii-Kosterlitz-Thouless Transition and its Application to Superconducting Systems* (2024).
- [14] V. Ambegaokar and L. P. Kadanoff, Electromagnetic properties of superconductors, *Il Nuovo Cimento* **22**, 914 (1961).
- [15] Y. Nambu, Quasi-particles and gauge invariance in the theory of superconductivity, *Phys. Rev.* **117**, 648 (1960).
- [16] Y. Nambu, Nobel lecture: Spontaneous symmetry breaking in particle physics: A case of cross fertilization, *Rev. Mod. Phys.* **81**, 1015 (2009).
- [17] P. Littlewood and C. Varma, Gauge-invariant theory of the dynamical interaction of charge density waves and superconductivity, *Phys. Rev. Lett.* **47**, 811 (1981).
- [18] A. A. Abrikosov, L. P. Gorkov, and I. E. Dzyaloshinski, *Methods of quantum field theory in statistical physics* (Courier Corporation, 2012).
- [19] J. Goldstone, Field theories with superconductor solutions, *Il Nuovo Cimento* **19**, 154 (1961).
- [20] J. Goldstone, A. Salam, and S. Weinberg, Broken symmetries, *Phys. Rev.* **127**, 965 (1962).
- [21] S. Fischer, M. Hecker, M. Hoyer, and J. Schmalian, Short-distance breakdown of the higgs mechanism and the robustness of the bcs theory for charged superconductors, *Phys. Rev. B* **97**, 054510 (2018).
- [22] i. c. v. Kos, A. J. Millis, and A. I. Larkin, Gaussian fluctuation corrections to the bcs mean-field gap amplitude at zero temperature, *Phys. Rev. B* **70**, 214531 (2004).
- [23] S. Mandal, S. Dutta, S. Basistha, I. Roy, J. Jesudasan, V. Bagwe, L. Benfatto, A. Thamizhavel, and P. Raychaudhuri, Destruction of superconductivity through phase fluctuations in ultrathin  $a$ -moge films, *Phys. Rev. B* **102**, 060501 (2020).
- [24] J. B. Curtis, N. Maksimovic, N. R. Poniatowski, A. Yacoby, B. Halperin, P. Narang, and E. Demler, Probing the berezinskii-kosterlitz-thouless vortex unbinding transition in two-dimensional superconductors using local noise magnetometry, *Phys. Rev. B* **110**, 144518 (2024).
- [25] L. Benfatto, C. Castellani, and T. Giamarchi, Broadening of the berezinskii-kosterlitz-thouless superconducting transition by inhomogeneity and finite-size effects, *Phys. Rev. B* **80**, 214506 (2009).
- [26] L. Benfatto, C. Castellani, and T. Giamarchi, Doping dependence of the vortex-core energy in bilayer films of cuprates, *Phys. Rev. B* **77**, 100506 (2008).
- [27] J. Yong, T. R. Lemberger, L. Benfatto, K. Ilin, and M. Siegel, Robustness of the berezinskii-kosterlitz-thouless transition in ultrathin nbn films near the superconductor-insulator transition, *Phys. Rev. B* **87**, 184505 (2013).
- [28] P. W. Anderson, Theory of dirty superconductors, *J. Phys. Chem. Solids* **11**, 26 (1959).
- [29] H. Suhl and B. Matthias, Impurity scattering in superconductors, *Phys. Rev.* **114**, 977 (1959).
- [30] S. Skalski, O. Betbeder-Matibet, and P. Weiss, Properties of superconducting alloys containing paramagnetic impurities, *Phys. Rev.* **136**, A1500 (1964).
- [31] L. Andersen, A. Ramires, Z. Wang, T. Lorenz, and Y. Ando, Generalized Anderson’s theorem for superconductors derived from topological insulators, *Sci. Adv.* **6**, eaay6502 (2020).
- [32] M. Silaev, Nonlinear electromagnetic response and higgs-mode excitation in bcs superconductors with impurities, *Phys. Rev. B* **99**, 224511 (2019).
- [33] F. Yang and M. W. Wu, Impurity scattering in superconductors revisited: Diagrammatic formulation of the supercurrent-supercurrent correlation and higgs-mode damping, *Phys. Rev. B* **106**, 144509 (2022).
- [34] G. Eilenberger, Transformation of gorkov’s equation for type ii superconductors into transport-like equations, *Z. Phys.* **214**, 195 (1968).
- [35] K. D. Usadel, Generalized diffusion equation for superconducting alloys, *Phys. Rev. Lett.* **25**, 507 (1970).
- [36] M. Tinkham, *Introduction to superconductivity*, Vol. 1 (Courier Corporation, 2004).
- [37] B. Sacépé, C. Chapelier, T. Baturina, V. Vinokur, M. Baklanov, and M. Sanquer, Disorder-induced inhomogeneities of the superconducting state close to the superconductor-insulator transition, *Phys. Rev. Lett.* **101**, 157006 (2008).
- [38] B. Sacépé, M. Feigel’man, and T. M. Klapwijk, Quantum breakdown of superconductivity in low-dimensional materials, *Nat. Phys.* **16**, 734 (2020).
- [39] B. Sacépé, T. Dubouchet, C. Chapelier, M. Sanquer, M. Ovadia, D. Shahar, M. Feigel’Man, and L. Ioffe, Localization of preformed Cooper pairs in disordered superconductors, *Nat. Phys.* **7**, 239 (2011).
- [40] D. Sherman, U. S. Pracht, B. Gorshunov, S. Poran, J. Jesudasan, M. Chand, P. Raychaudhuri, M. Swanson, N. Trivedi, A. Auerbach, *et al.*, The Higgs mode in disordered superconductors close to a quantum phase transition, *Nat. Phys.* **11**, 188 (2015).
- [41] T. Dubouchet, B. Sacépé, J. Seidemann, D. Shahar, M. Sanquer, and C. Chapelier, Collective energy gap of preformed Cooper pairs in disordered superconductors, *Nat. Phys.* **15**, 233 (2019).
- [42] D. C. Mattis and J. Bardeen, Theory of the anomalous skin effect in normal and superconducting metals, *Phys. Rev.* **111**, 412 (1958).
- [43] S. B. Nam, Theory of electromagnetic properties of superconducting and normal systems. I, *Phys. Rev.* **156**, 470 (1967).
- [44] T. R. Lemberger, I. Hetel, J. W. Knepper, and F. Y. Yang, Penetration depth study of very thin superconducting nb films, *Phys. Rev. B* **76**, 094515 (2007).
- [45] A. I. Gubin, K. S. Il’in, S. A. Vitusevich, M. Siegel, and N. Klein, Dependence of magnetic penetration depth on the thickness of superconducting nb thin films, *Phys. Rev. B* **72**, 064503 (2005).
- [46] C. Varmazis and M. Strongin, Inductive transition of niobium and tantalum in the 10-mhz range. i. zero-field superconducting penetration

depth, Phys. Rev. B **10**, 1885 (1974).

[47] G. E. Peabody and R. Meservey, Magnetic flux penetration into superconducting thin films, Phys. Rev. B **6**, 2579 (1972).

[48] L. D. Landau, E. M. Lifshitz, and L. P. Pitaevskii, *Statistical Physics, Part 1* (Pergamon, New York, 1980).

[49] L. Benfatto, A. Toschi, S. Caprara, and C. Castellani, Phase fluctuations in superconductors: From galilean invariant to quantum XY models, Phys. Rev. B **64**, 140506 (2001).

[50] L. Benfatto, A. Toschi, and S. Caprara, Low-energy phase-only action in a superconductor: A comparison with the XY model, Phys. Rev. B **69**, 184510 (2004).

[51] C. Verdi, L. Ranalli, C. Franchini, and G. Kresse, Quantum paraelectricity and structural phase transitions in strontium titanate beyond density functional theory, Phys. Rev. Mater. **7**, L030801 (2023).

[52] H. Wu, R. He, Y. Lu, and Z. Zhong, Large-scale atomistic simulation of quantum effects in  $\text{SrTiO}_3$  from first principles, Phys. Rev. B **106**, 224102 (2022).

[53] M. E. Peskin, *An introduction to quantum field theory* (CRC press, 2018).

[54] K. A. Müller and H. Burkard,  $\text{SrTiO}_3$ : An intrinsic quantum paraelectric below 4 K, Phys. Rev. B **19**, 3593 (1979).

[55] X. Li, T. Qiu, J. Zhang, E. Baldini, J. Lu, A. M. Rappe, and K. A. Nelson, Terahertz field-induced ferroelectricity in quantum paraelectric  $\text{SrTiO}_3$ , Science **364**, 1079 (2019).

[56] B. Cheng, P. L. Kramer, Z.-X. Shen, and M. C. Hoffmann, Terahertz-driven local dipolar correlation in a quantum paraelectric, Phys. Rev. Lett. **130**, 126902 (2023).

[57] Y. Jia, P. Wang, C.-L. Chiu, Z. Song, G. Yu, B. Jäck, S. Lei, S. Klemenz, F. A. Cevallos, M. Onyszczak, N. Fishchenko, X. Liu, G. Farahi, F. Xie, Y. Xu, K. Watanabe, T. Taniguchi, B. A. Bernevig, R. J. Cava, L. M. Schoop, A. Yazdani, and S. Wu, Evidence for a monolayer excitonic insulator, Nature Physics **18**, 87 (2022).

[58] V. Fatemi, S. Wu, Y. Cao, L. Bretheau, Q. D. Gibson, K. Watanabe, T. Taniguchi, R. J. Cava, and P. Jarillo-Herrero, Electrically tunable low-density superconductivity in a monolayer topological insulator, Science **362**, 926 (2018).

[59] E. Sajadi, T. Palomaki, Z. Fei, W. Zhao, P. Bement, C. Olsen, S. Luescher, X. Xu, J. A. Folk, and D. H. Cobden, Gate-induced superconductivity in a monolayer topological insulator, Science **362**, 922 (2018).

[60] T. Song, Y. Jia, G. Yu, Y. Tang, P. Wang, R. Singha, X. Gui, A. J. Uzan-Narovlansky, M. Onyszczak, K. Watanabe, *et al.*, Unconventional superconducting quantum criticality in monolayer  $\text{WTe}_2$ , Nat. Phys. **20**, 269 (2024).

[61] T. Song, Y. Jia, G. Yu, Y. Tang, A. J. Uzan, Z. J. Zheng, H. Guan, M. Onyszczak, R. Singha, X. Gui, K. Watanabe, T. Taniguchi, R. J. Cava, L. M. Schoop, N. P. Ong, and S. Wu, Unconventional superconducting phase diagram of monolayer  $\text{WTe}_2$ , Phys. Rev. Res. **7**, 013224 (2025).

[62] G. Kresse and J. Furthmüller, Efficiency of ab-initio total energy calculations for metals and semiconductors using a plane-wave basis set, Comp. Mater. Sci. **6**, 15 (1996).

[63] G. Kresse and J. Furthmüller, Efficient iterative schemes for ab initio total-energy calculations using a plane-wave basis set, Phys. Rev. B **54**, 11169 (1996).

[64] J. P. Perdew, K. Burke, and M. Ernzerhof, Generalized gradient approximation made simple, Phys. Rev. Lett. **77**, 3865 (1996).

[65] S. Grimme, S. Ehrlich, and L. Goerigk, Effect of the damping function in dispersion corrected density functional theory, J. Comput. Chem. **32**, 1456 (2011).

[66] X. Liu, Y. Yang, T. Hu, G. Zhao, C. Chen, and W. Ren, Vertical ferroelectric switching by in-plane sliding of two-dimensional bilayer  $\text{WTe}_2$ , Nanoscale **11**, 18575 (2019).

[67] B. Sun, W. Zhao, T. Palomaki, Z. Fei, E. Runburg, P. Malinowski, X. Huang, J. Cenker, Y.-T. Cui, J.-H. Chu, X. Xu, S. S. Ataei, D. Varsano, M. Palummo, E. Molinari, M. Rontani, and D. H. Cobden, Evidence for equilibrium exciton condensation in monolayer  $\text{WTe}_2$ , Nat. Phys. [10.1038/s41567-021-01427-5](https://doi.org/10.1038/s41567-021-01427-5) (2021).